
SGS-GNN: A Supervised Graph Sparsifier for Graph Neural Networks

Siddhartha Shankar Das¹ Naheed Anjum Arafat² Muftiqur Rahman³ S M Ferdous⁴ Alex Pothan¹
Mahantesh M Halappanavar⁴

Abstract

We propose *SGS-GNN*, a novel supervised graph sparsifier that learns the sampling probability distribution of edges and samples sparse subgraphs of a user-specified size to reduce the computational costs required by GNNs for inference tasks on large graphs. *SGS-GNN* employs regularizers in the loss function to enhance homophily in sparse subgraphs, boosting the accuracy of GNNs on heterophilic graphs, where a significant number of the neighbors of a node have dissimilar labels. *SGS-GNN* also supports conditional updates of the probability distribution learning module based on a prior, which helps narrow the search space for sparse graphs. *SGS-GNN* requires fewer epochs to obtain high accuracies since it learns the search space of subgraphs more effectively than methods using fixed distributions such as random sampling. Extensive experiments using 33 homophilic and heterophilic graphs demonstrate the following: (i) with only 20% of edges retained in the sparse subgraphs, *SGS-GNN* improves the F1-scores by a geometric mean of 4% relative to the original graph; on heterophilic graphs, the prediction accuracy is better up to 30%. (ii) *SGS-GNN* outperforms state-of-the-art methods with improvement in F1-scores of 4 – 7% in geometric mean with similar sparsities in the sampled subgraphs, and (iii) compared to sparsifiers that employ fixed distributions, *SGS-GNN* requires about half the number of epochs to converge.

1 Introduction

Given a graph $\mathcal{G} \triangleq (\mathcal{V}, \mathcal{E}, \mathbf{X})$ with node features \mathbf{X} , the goal of a graph neural network (GNN) with hidden dimen-

¹Department of Computer Science, Purdue University, West Lafayette, IN 47907, USA ²Independent Researcher, USA ³Islamic University of Technology, Dhaka, Bangladesh ⁴Pacific Northwest National Lab, Richland, WA, USA. Correspondence to: Siddhartha Shankar Das <das90@purdue.edu>, Naheed Anjum Arafat <naheed.anjum@u.nus.edu>.

sion H is to learn an encoding $\mathbf{h}_v \in \mathbb{R}^H$ of each node $v \in \mathcal{V}$ that encodes the neighborhood information of v . The encoding \mathbf{h}_v is used to compute an output \mathbf{y}_v for a variety of predictive tasks (detailed in §2). GNNs (Wu et al., 2022; Zhou et al., 2020) are effective tools for learning from graph-structured data, utilized in areas like social networks (Wu et al., 2021), biological networks (Muzio et al., 2021), computational physics (Jessica et al., 2024), and recommender systems (Yu et al., 2022). However, their computational and memory demands can be substantial, particularly for large graphs. The two primary steps in a Graph Neural Network (GNN) are *aggregation* and *update*. For each node, the aggregation step involves accumulating embeddings from neighboring nodes using sparse matrix operations such as sparse-matrix dense-matrix multiplication (SpMM) and sampled dense-matrix dense-matrix multiplication (SDDMM) (Zhang et al., 2024). During the update step, a node updates its own embedding based on the aggregated information using dense matrix operations (MatMul) (Zhang et al., 2024). Approximately 70% of the total cost is attributed to the SpMM operations (Liu et al., 2023). Thus, by systematically removing nonessential edges, *graph sparsification* (Chen et al., 2023; Hashemi et al., 2024) reduces computational costs and memory requirements, and significantly speeds up GNN training and inference.

A sparse subgraph $\tilde{\mathcal{G}} \triangleq (\mathcal{V}, \tilde{\mathcal{E}}, \mathbf{X})$ contains at most $q\%$ of original edges, $\tilde{\mathcal{E}} \subseteq \mathcal{E}$ (defined in §2; q is an input parameter). A graph can be sparsified using two broad approaches: unsupervised and supervised. Unsupervised graph sparsification methods, such as spectral sparsification (Batson et al., 2013) and spanners (Dragan et al., 2011), only focus on the structural characteristics of graphs, neglecting downstream tasks and the differences between homophilic (similar nodes connect) and heterophilic graphs (dissimilar nodes connect). This oversight can result in sparsified graphs that do not effectively support tasks like node classification or link prediction (Zheng et al., 2020). In contrast, supervised graph sparsification methods (Zheng et al., 2020) aim to reduce graph complexity while maintaining relevance to downstream tasks (Luo et al., 2021; Wu et al., 2023; Ye & Ji, 2021). Methods such as SparseGAT (Ye & Ji, 2021) and SuperGAT (Kim & Oh, 2022) are considered *implicit sparsifiers* as they do not create a standalone sparse subgraph for

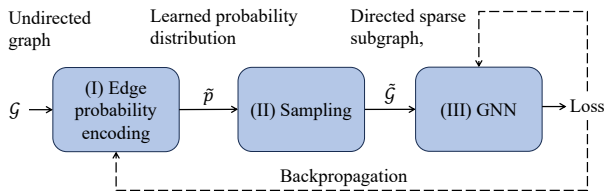


Figure 1: Simplified architecture of SGS-GNN.

independent use, and thus they do not reduce GNN memory requirements. In contrast, NeuralSparse (Zheng et al., 2020) is an *explicit sparsifier* that constructs a subgraph based on a neighborhood size, but this approach can lack precise control over sparsity and may retain unnecessary edges. The vast search space for sparse subgraphs makes it hard for supervised sparsifiers to find an optimal sampling distribution within limited iterations. Further, sparsifier modules can be compute-intensive with limited support for batch processing.

To address these limitations, we propose SGS-GNN (§4), a fast and lightweight supervised graph sparsifier that learns the edge probability distribution of an input graph to construct a sparse subgraph for downstream GNNs. SGS-GNN consists of three components (Fig. 1): (i) edge probability encoding, (ii) sparse subgraph sampler, and (iii) downstream GNN. The edge probability encoding, called EdgeMLP, maps associated node features of edges into probabilities indicating the likelihood of specific edges to exist in the learned sparse subgraph. The subgraph sampler then samples a subgraph based on these learned probabilities. *Finally, the GNN can be any message passing through a neural network.* SGS-GNN provides a unique advantage by allowing the downstream GNN to operate solely on a reduced sparse graph instead of the input graph and supports batch processing for large graphs. In addition to the task-specific loss, one of the regularizers promotes homophily in sampled subgraphs, enhancing prediction quality in heterophilic scenarios. The key contributions of our work are:

1. We propose a novel graph sparsification technique, SGS-GNN, that works for both homophilic and heterophilic graphs (§4). With SGS-GNN, users can control the amount of sparsity, efficiently learn sampling probabilities, and scale to large graphs with batch processing. SGS-GNN incorporates degree-proportionate edge weight as *prior* sampling distribution to guide the search for sparse subgraphs. The conditional update module in SGS-GNN encodes edge probabilities to further optimize performance and adaptability.
2. We provide theoretical bounds and empirical validation for SGS-GNN, ensuring quality of the learned embeddings.
3. Extensive experiments on 33 benchmark graphs (21 heterophilic, 12 homophilic) show that SGS-GNN outperforms almost all original dense heterophilic graphs with up to 30% improvement in F1-scores (on a scale of 100) using only

20% of the edges (§5.1.1). In homophilic graphs, SGS-GNN remains competitive. In similar settings, SGS-GNN outperforms sparsification-based GNN methods such as GraphSAINT (Zeng et al., 2019), NeuralSparse (Zheng et al., 2020), SparseGAT (Ye & Ji, 2021), MOG (Zhang et al., 2024), DropEdge (Rong et al., 2019), with geometric mean improvement of 4 – 7% in F1-scores.

4. Additionally, EdgeMLP surpasses fixed distribution sparsifiers and requires fewer epochs. SGS-GNN is significantly faster than related supervised sparsifiers (§5.1.5).

2 Preliminaries

$\mathcal{G} \triangleq (\mathcal{V}, \mathcal{E}, \mathbf{X})$ is an undirected graph with its set of nodes and edges denoted by \mathcal{V} and \mathcal{E} respectively. The node feature matrix $\mathbf{X} \in \mathbb{R}^{|\mathcal{V}| \times F}$ contains node feature $\mathbf{x}_v \in \mathbb{R}^F$ as a row vector for every node $v \in \mathcal{V}$. The adjacency matrix $\mathbf{A}_{\mathcal{G}}$ of size $|\mathcal{V}| \times |\mathcal{V}|$ captures the neighborhood of each node in \mathcal{G} . In node classification, the goal is to predict a label $y_v \in C$ for each node $v \in \mathcal{V}$ among the $|C|$ possible class labels. The training uses labeled nodes $\mathcal{V}_L \subset \mathcal{V}$, while the unlabeled nodes $\mathcal{V}_U = \mathcal{V} \setminus \mathcal{V}_L$ are used for validation and testing. A single-layer Graph Convolutional Network (GCN) (Kipf & Welling, 2016) is defined as:

$$\mathbf{H}^{(l+1)} = \sigma(\hat{\mathbf{A}}_{\mathcal{G}} \mathbf{H}^{(l)} \mathbf{W}^{(l)}), \quad (1)$$

where $\mathbf{H}^{(l)}$ represents the node embedding at layer l , with $\mathbf{H}^{(0)} = \mathbf{X}$, and $\mathbf{W}^{(l)}$ is the learnable weight matrix in layer l . $\hat{\mathbf{A}}_{\mathcal{G}}$ denotes the normalized adjacency matrix and σ is an activation function such as ReLU. The predicted probabilities can be expressed as $\hat{\mathbf{Y}} = \text{Softmax}(f_{\text{GNN}, \theta}(\mathcal{G}))$ where $f_{\text{GNN}, \theta}(\mathcal{G})$ is a GCN model with L layers and learnable parameters θ . The dimension of $\hat{\mathbf{Y}}$ is $|\mathcal{V}| \times |C|$. The training objective is to find parameters θ that minimize the cross-entropy loss,

$$\mathcal{L}_{\text{CE}} = -\frac{1}{|\mathcal{V}_L|} \sum_{v \in \mathcal{V}_L} \sum_{c=1}^{|C|} Y_{vc} \log \hat{Y}_{vc}, \quad (2)$$

where Y_{vc} indicates the true probability of node v belonging to class $c \in C$.

The *homophily* of a graph characterizes the likelihood that nodes with the same labels are neighbors. Two commonly used measures are *Node homophily* \mathcal{H}_n (Pei et al., 2020) and *Edge homophily* \mathcal{H}_e (Zhu et al., 2020) and defined as

$$\mathcal{H}_n = \frac{1}{|\mathcal{V}|} \sum_{u \in \mathcal{V}} \frac{|\{v \in \mathcal{N}(u) : y_v = y_u\}|}{|\mathcal{N}(u)|}, \quad (3)$$

$$\mathcal{H}_e = \frac{|\{(u, v) \in \mathcal{E} : y_u = y_v\}|}{|\mathcal{E}|}. \quad (4)$$

The values of \mathcal{H}_n and \mathcal{H}_e range from 0 to 1, where a value close to 1 indicates strong homophily, and a value close to 0 indicates strong heterophily.

2.1 Problem Statement and Theoretical Motivation

Given $q > 0$, this paper aims to construct a sparse subgraph $\tilde{\mathcal{G}} \triangleq (\mathcal{V}, \tilde{\mathcal{E}}, \mathbf{X})$ with $q\%$ of original edges in \mathcal{E} . Let \mathcal{G}_q be the space of all distinct sparse subgraphs of \mathcal{G} where every subgraph contains exactly $k = \lfloor \frac{q|\mathcal{E}|}{100} \rfloor$ edges, $\mathcal{G}_q = \{\tilde{\mathcal{E}} \subset \mathcal{E} : |\tilde{\mathcal{E}}| = k\}$. The objective of our supervised sparse graph construction is to find the parameters θ along with a sparse subgraph $\tilde{\mathcal{G}} \in \mathcal{G}_q$ that minimize \mathcal{L}_{CE} .

We can define a probability space (Ω, \mathcal{F}, p) by considering \mathcal{E} as the sample space, $\mathcal{F} = \mathcal{G}_q \subseteq 2^\Omega$ as the event space and a suitable probability measure $p : \mathcal{F} \rightarrow [0, 1]$. The probability measure is determined by which subgraphs result in a node representation that minimizes the loss in Eq. 2, which, in turn, depends on the downstream task. As a result, it is unknown which probability distribution is suitable as a choice for p . Specifically, we can perform the following decomposition to predict the probability that a node v belongs to a class $c \in C$,

$$P(\tilde{Y}_{vc}|\mathcal{G}) = \sum_{\tilde{\mathcal{G}} \in \mathcal{G}_q} P(\tilde{Y}_{vc}|\tilde{\mathcal{G}})P(\tilde{\mathcal{G}}|\mathcal{G}). \quad (5)$$

There are two issues with the above decomposition. First, it requires enumerating all possible candidate subgraphs $\tilde{\mathcal{G}} \in \mathcal{G}_q$. This is computationally challenging because there are $\binom{|\mathcal{E}|}{k}$ subgraphs, and it is not possible to estimate the probabilities $P(\tilde{Y}_{vc}|\tilde{\mathcal{G}})$, $P(\tilde{\mathcal{G}}|\mathcal{G})$ due to their dependence on the downstream task under consideration.

We address these issues by encoding $P(\tilde{\mathcal{G}}|\mathcal{G})$ as a learnable neural network module $\tilde{p} = f_{\text{EdgeMLP}, \phi}(\mathcal{G})$ that explicitly learns to estimate the probability measure p for every edge based on the downstream task. The neural network searches the space \mathcal{G}_q by adjusting its learned probability estimate \tilde{p} based on the gradient of the loss. Finally, we model $P(\tilde{Y}_{vc}|\tilde{\mathcal{G}})$ as a GNN that takes the sparsified sample $\tilde{\mathcal{G}}$ sampled from the learned distribution \tilde{p} . Hence, Eq. 5 can be approximated by,

$$P(\tilde{Y}_{vc}|\mathcal{G}) \approx \mathbb{E}_{\tilde{\mathcal{G}} \sim f_{\text{EdgeMLP}, \phi}(\mathcal{G})} [f_{\text{GNN}, \theta}(\tilde{\mathcal{G}}) f_{\text{EdgeMLP}, \phi}(\mathcal{G})]. \quad (6)$$

Equation 6 follows since instead of directly searching over the space \mathcal{G}_q , we rely on the distribution \tilde{p} approximated via a neural network. Once this distribution is learned, the law of large numbers indicates that a sufficient number of samples from $\tilde{\mathcal{G}} \sim \tilde{p}$ can estimate $P(\tilde{Y})$. Thus the summation can be replaced with the expected value from a learned GNN model using sparse subgraph samples.

3 Related Work

Unsupervised Graph Sparsification. Effective resistance (ER) (Spielman & Srivastava, 2011) based sampling generates spectral sparse subgraphs while bounding the eigenvalues of the original graph’s Laplacian. FastGAT (Srinivasa

et al., 2020) uses ER to improve GNN efficiency, but the high computational cost of ER makes it impractical for large graphs. However, a major advantage of ER is its ability to produce multiple sparse subgraphs, minimizing information loss and improving GNN performance compared to single sparse graph methods such as k -NN. The random sparsifier is the fastest approach to get sparse subgraphs and is widely used in GNNs such as DropEdge (Rong et al., 2019) and GraphSAGE (Hamilton et al., 2017). GraphSAINT (Zeng et al., 2019) uses the normalized *degree* as edge weight to assign low sampling probability to edges in denser clusters. Later, it is used for sampling subgraphs and often produces better results than random sparsifiers. Spanner (e.g., t -spanner) (Dragan et al., 2011) is a topology-based sparsifier that preserves distances between nodes in a sparse subgraph by a factor of t . Spanning Tree and Forest are useful sparsifiers, as they preserve node connectivity, which helps message propagation in GNNs. Although both of these lack control over sparsity, the notion of connectivity is essential. Some other topology-based sparsifiers include Rank Degree Sparsifier (Voudigari et al., 2016), Local Degree Sparsifier (Hamann et al., 2016), Forest Fire (Leskovec et al., 2007), and Degree-based sparsification (Su et al., 2024; Liu et al., 2023). Another class of unsupervised sparsifiers first computes similarities between two nodes as edge weight and then samples. It could be structural similarity, such as *Jaccard distance* on a portion of shared neighbors (SCAN (Xu et al., 2007)) or feature similarity (SimSparse (Wu et al., 2023), AGS-GNN (Das et al., 2024)).

Supervised Graph Sparsification. Supervised graph sparsification may have computational overhead due to their training phase but is often compensated by prediction quality in noisy or heterophilic graphs. Methods like SparseGAT (Ye & Ji, 2021) and SuperGAT (Kim & Oh, 2022) use the entire graph information during GNN training and learn sparse subgraphs through regularizers. SGCN (Li et al., 2020) is another sparsification method that optimizes the runtime by alternating the sparsifier’s and GNN’s learning. NeuralSparse (Zheng et al., 2020), PDTNet (Luo et al., 2021), explicitly learn to sample sparse subgraphs. Ours SGS-GNN falls into a similar category with distinctions. NeuralSparse samples k -neighbors from each node to generate the sparse graphs, whereas SGS-GNN globally learns the sampling distribution of all edges and then samples from that distribution, which is significantly faster. SGS-GNN uses a prior probability distribution to narrow the sparse subgraph search space; this notion of prior is useful (Wang et al., 2024) and recent work like Mixture of Graphs (MOG) (Zhang et al., 2024) uses *Jaccard similarity*, *gradient magnitude*, and *effective resistance* as prior for sparse subgraph selection. Additionally, LAGCN (Chen et al., 2020) employs an edge classifier to modify graphs based on training nodes, while our EdgeMLP coupled with regularizer uses training

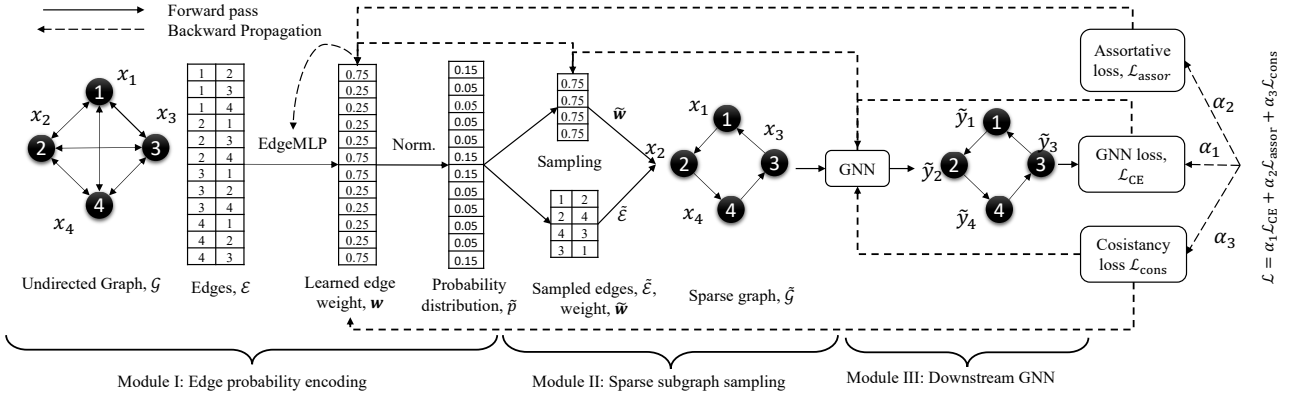


Figure 2: Illustration of the three modules in SGS-GNN. The edge probability encoding module computes a probability distribution, the sampler module samples the subgraph, and downstream GNN makes predictions using that sparse subgraph.

edges to foster homophily in the sampled subgraph.

4 Proposed method: SGS-GNN

Figure 2 depicts our proposed method SGS-GNN. In the following, we discuss its major components.

4.1 Module I: Edge Probability Encoding

Given input \mathcal{G} , the edge probability encoding module (EdgeMLP) maps the node features to edge weights in the range $[0, 1]$ followed by normalization to turn the learned weights into probabilities. The learned edge weights represent the model’s unnormalized confidence in the existence of each edge. EdgeMLP learns the edge weights of (u, v) as a function of node embeddings $\mathbf{h}_u, \mathbf{h}_v$:

$$w(e_{uv}) = \sigma(\text{MLP}_\phi((\mathbf{h}_u - \mathbf{h}_v) \oplus (\mathbf{h}_u \odot \mathbf{h}_v))). \quad (7)$$

Here, σ refers to Sigmoid activation function, \oplus indicates concatenation, and \odot represents element-wise multiplication. Let us assume \mathbf{h}_u indicates the node embedding in matrix \mathbf{H} corresponding to node u . Thus the node embedding matrix \mathbf{H} can be computed from an MLP in the following manner: $\mathbf{H} = \text{ReLU}(\text{MLP}_{\mathbf{W}}(\mathbf{X}))$, where $\text{MLP}_{\mathbf{W}}$ is an MLP with weights \mathbf{W} . MLP is computationally efficient; however, it does not exploit the graph structural information. As a result, MLP is not necessarily the most effective choice, as we have shown later in the Ablation study (section F).

A common way to incorporate graph structural information is to use graph convolutions such as vanilla GCN (Kipf & Welling, 2016) or SAGE convolution (Hamilton et al., 2017). For instance, one can compute graph-structure aware node embedding matrix using a single-layer GCN as the following: $\mathbf{H} = \sigma(\hat{\mathbf{A}}_{\mathcal{G}} \mathbf{X} \mathbf{W})$, where \mathbf{W} is the learnable weight matrix. However, considering the entire graph $\mathbf{A}_{\mathcal{G}}$ is memory intensive for large graphs.

Thus SGS-GNN takes a length $\lfloor \frac{q|\mathcal{E}|}{100} \rfloor$ subset of edges $\mathcal{E}_{\text{sp}} \subseteq \mathcal{E}$ following a fixed prior probability distribution p_{prior} and uses the induced subgraph $\mathcal{G}[\mathcal{E}_{\text{sp}}]$ for computing node embedding \mathbf{H} . In order to maintain good connectivity in $\mathcal{G}[\mathcal{E}_{\text{sp}}]$, the prior distribution is defined as the following: $\forall (u,v) \in \mathcal{E} p_{\text{prior}}(u, v) \propto (\frac{1}{d_u} + \frac{1}{d_v})$, where d_u, d_v are the degrees of nodes u, v .

Normalization. Normalization turns the learned edge weights into a valid probability distribution. One simple choice is *sum-normalization* computed as following: $\tilde{p}(e_{uv}) = w(e_{uv}) / \sum_{(u,v) \in \mathcal{E}} w(e_{uv})$. Another choice is *softmax-normalization* with temperature annealing,

$$\tilde{p}(e_{uv}) = \frac{\exp(w(e_{uv})/T)}{\sum_{(u,v) \in \mathcal{E}} \exp(w(e_{uv})/T)}. \quad (8)$$

Here, $T > 0$ is the temperature parameter. When T is large, the learned distribution \tilde{p} approaches uniform distribution over edges, whereas the learned distribution \tilde{p} approaches categorical distribution when T is small (Jang et al., 2016). As the learned distribution approaches uniform distribution, the model tends to explore more diverse subgraphs from subgraph space \mathcal{G}_q . On the other hand, as the learned distribution approaches categorical distribution, the model tends to explore less in \mathcal{G}_q . Hence, we vary T as a function of training iterations such that in early iterations, the algorithm explores more while narrowing down to its preferred search space later on. We execute such an annealing mechanism with the following equation:

$$T = \max(T_{\min}, T_0 - \text{epoch} \cdot r), \quad (9)$$

where $r = (T_0 - T_{\min}) / \text{max_epochs}$ is the annealing rate, T_{\min} is the minimum allowable temperature, and T_0 is the initial temperature. The temperature linearly decreases from the initial value T_0 to its final value T_{\min} with the epochs. We keep track of the T -value that gives the best validation accuracy and use it later during inference.

Alg. 1 shows the pseudocode for EdgeMLP.

Algorithm 1 EdgeMLP Module

- 1: **Input:** $\mathcal{G}(\mathcal{V}, \mathcal{E}, \mathbf{X})$, sample % q , #layers L , epoch, max_epochs
 - 2: $\forall_{(u,v) \in \mathcal{E}} p_{\text{prior}}(u, v) \leftarrow \frac{1/d_u + 1/d_v}{\sum_{i,j \in \mathcal{E}} (1/d_i + 1/d_j)}$
 - 3: $\mathcal{E}_{\text{sp}} \leftarrow \text{Multinomial}(\mathcal{E}, p_{\text{prior}}, \lfloor \frac{q|\mathcal{E}|}{100} \rfloor)$
 - 4: $\mathbf{H} \leftarrow \text{GCN}_W(\mathcal{E}_{\text{sp}}, \mathbf{X}, L)$
 - 5: $\forall_{(u,v) \in \mathcal{E}} \mathbf{w}(u, v) = \sigma_{\text{MLP}_\phi}((\mathbf{h}_u^{(i)} - \mathbf{h}_v^{(i)}) \oplus (\mathbf{h}_u^{(i)} \odot \mathbf{h}_v^{(i)}))$
 - 6: $T \leftarrow \max(T_{\text{min}}, T_0 - \text{epoch} \cdot \frac{T_0 - T_{\text{min}}}{\text{max_epochs}})$
 - 7: $\tilde{p} \leftarrow \text{Softmax}(\mathbf{w}/T)$
 - 8: **Return** \tilde{p}, \mathbf{w}
-

4.2 Module II: Sparse Subgraph Sampling

Given the learned distribution \tilde{p} over the edges of the input graph, sparse subgraph sampling aims to construct a sparse graph with the user-given sparsity constraint q . We do not know which discrete distribution has \tilde{p} as parameters. A natural choice is to construct $\tilde{\mathcal{G}} = (\mathcal{V}, \tilde{\mathcal{E}}, \mathbf{X})$ by assuming that \tilde{p} is a parameter of a *Multinomial* distribution. Hence we can sample $k = \lfloor \frac{q|\mathcal{E}|}{100} \rfloor$ edges as $\tilde{\mathcal{E}} \sim \text{Multinomial}(\tilde{p}, k)$.

We can also construct $\tilde{\mathcal{G}}$ by assuming that \tilde{p} is a parameter of some categorical distribution and use *Gumbel Softmax trick* (Jang et al., 2016). The idea is to induce *Gumbel noise* $g_{uv} \sim \text{Gumbel}(0, 1)$ to the edges and select Top- K edges with the highest probabilities. In order to sample edges according to categorical distribution, we replace our softmax-normalization (Equation 8) with the following:

$$\tilde{p}(e_{uv}) = \frac{\exp((\log w(e_{uv}) + g_{uv})/T)}{\sum_{(u,v) \in \mathcal{E}} \exp((\log w(e_{uv}) + g_{uv})/T)}. \quad (10)$$

Adding noise ensures that we are taking different samples at each time, and with low temperatures ($T = 0.1, T = 0.5$), the samples become identical to samples from a categorical distribution (Jang et al., 2016).

Theoretical analysis I. Let \mathcal{E}^* and $\tilde{\mathcal{E}}$ denote the ordered collection of edges sampled by the idealized learning ORACLE according to true distribution p^* and by SGS-GNN according to learned probability \tilde{p} respectively. For analytical convenience, let us assume that the algorithm samples k edges with replacement. We have the following theorem that lower-bounds the #edges common between sampled subgraphs from SGS-GNN and idealized learning ORACLE.

Theorem 4.1 (Lower-bound). *The expected number of edges sampled by both SGS-GNN and idealized learning ORACLE satisfies*

$$\mathbb{E}[|\mathcal{E}^* \cap \tilde{\mathcal{E}}|] \geq k \sum_{j=1}^{|\mathcal{E}|} \frac{(p_j^* + \tilde{p}_j - \epsilon)^2}{4}, \quad (11)$$

where $k = \lfloor q|\mathcal{E}|/100 \rfloor$ with $0 \leq q \leq 100$ as a user-specified parameter and $\epsilon \in [0, 1]$ is the error.

The proof is in Appendix A.2. The implications are:

1. Let the true distribution be uniform. In the best-case scenario $\epsilon \rightarrow 0$ and $\tilde{p} = p^* = \frac{1}{|\mathcal{E}|}$. Then there are at least $\frac{k}{|\tilde{\mathcal{E}}|}$ common edges between $\tilde{\mathcal{G}}$ and \mathcal{G}^* . Since $k \ll |\mathcal{E}|$, this specific scenario suggests that the learned sparse subgraph may not overlap much with the true one even after we have learned the true distribution. When the true distribution is uniform, every subgraph from \mathcal{G}_q is a global minimizer of the task-specific loss \mathcal{L}_{CE} . Otherwise, the learning ORACLE would have put more mass on certain edges and the distribution p^* would not have been uniform. As individual subgraphs are indistinguishable in terms of performance, this case beats the purpose of supervised sparsification.

2. Let the true distribution be one-hot. In other words, suppose $\tilde{p} = p^* = \delta_{ij}$, where δ_{ij} is the *Kronecker-delta*. In this case, as $\epsilon \rightarrow 0$, the lower bound reduces to

$$\mathbb{E}[|\mathcal{E}^* \cap \tilde{\mathcal{E}}|] \geq k \sum_{j=1}^{|\mathcal{E}|} (\tilde{p}_j)^2 = k.$$

This identity suggests that the sampled edges are expected to completely overlap with the true sparse subgraph.

For strong heterophilic graphs (\mathcal{H}_n is small), the true distribution is less likely to be uniform. Because a uniform edge sample would retain a similar node homophily as in the input graph, and such a subgraph would not be able to minimize \mathcal{L}_{CE} (Das et al., 2024). Thus, it is important for the learned probability distribution to approximate p^* so that the sampled subgraph is close enough to the true one.

We have analyzed $\tilde{\mathcal{G}}$ generated by SGS-GNN on a synthetic graph in Appendix B.

4.3 Module III: Downstream GNN and Loss Functions

At this stage, we input the sampled subgraph to a downstream GNN that supports edge weights as computed in Equation 7; since the edge weights of the sampled edges are one of the ways we optimize EdgeMLP via backpropagation. An example GNN would be

$$\hat{\mathbf{Y}} = \text{Softmax}(f_{\text{GNN}, \theta}(\mathcal{V}, \tilde{\mathcal{E}}, \mathbf{X}, \tilde{\mathbf{w}})), \quad (12)$$

where $\tilde{\mathcal{E}}$ refers to the edges of the sampled sparse subgraph \mathcal{G}' and $\tilde{\mathbf{w}} = \mathbf{w}[\tilde{\mathcal{E}}]$ contains the edge weights.

Loss functions. We introduce two regularizers to engrain various inductive biases to SGS-GNN and combined these functions with the Cross-Entropy loss \mathcal{L}_{CE} as follows:

$$\mathcal{L} = \alpha_1 \mathcal{L}_{CE} + \alpha_2 \mathcal{L}_{\text{assor}} + \alpha_3 \mathcal{L}_{\text{cons}}, \quad (13)$$

where $0 \leq \alpha_1, \alpha_2, \alpha_3 \leq 1$ are regularizer coefficients.

The **Assortativity loss** $\mathcal{L}_{\text{assor}}$ uses the labels of the training nodes to force nodes with similar labels to have higher edge weights while forcing dissimilarly labeled nodes to have

a small nonzero weight. This regularizer encourages edge homophily in the sampled sparse graph.

$$\mathcal{L}_{\text{assor}} \triangleq - \sum_{(u,v) \in \mathcal{E}: u \wedge \mathcal{V}_L \wedge v \in \mathcal{V}_L} \mathbb{I}(y_u = y_v) \cdot \log w(e_{uv}), \quad (14)$$

where $\mathbb{I}(\cdot)$ is an indicator function that returns 0 or 1.

The **Consistency loss** defined below encourages learned edge probabilities to reflect the similarity between node embeddings or features:

$$\mathcal{L}_{\text{cons}} \triangleq \sum_{(u,v) \in \tilde{\mathcal{E}}} \|w(e_{uv}) - \text{cosine}(\mathbf{h}_u^l, \mathbf{h}_v^l)\|, \quad (15)$$

where $\text{cosine}(\mathbf{h}_u^l, \mathbf{h}_v^l) = \mathbf{h}_u^l \cdot \mathbf{h}_v^l / \|\mathbf{h}_u^l\| \|\mathbf{h}_v^l\|$ is the cosine similarity of the learned GNN embeddings $\mathbf{h}_u^l, \mathbf{h}_v^l$ of nodes u, v from layer l , and $w(e_{uv})$ is the learned probability for edge (u, v) in the sparse graph $\tilde{\mathcal{G}}$. This mechanism aligns the edge probabilities with the global graph structure and ensures that the sparsifier learns to preserve edges consistent with the broader graph relationships.

Theoretical analysis II. We consider vanilla GCN as a downstream GNN to examine how the sparse subgraph, $\tilde{\mathcal{G}}$ from SGS-GNN, affects node embeddings compared to the ideal subgraph \mathcal{G}^* from a learning ORACLE. Suppose an L -layer GCN produces embeddings $\tilde{\mathbf{H}}^{(L)}$ and $\mathbf{H}^{*(L)}$ when taking $\tilde{\mathcal{G}}$ and \mathcal{G}^* as input, respectively. Is there an upper bound of the difference in the downstream node encodings $\mathbb{E}[\|\tilde{\mathbf{H}}^{(L)} - \mathbf{H}^{*(L)}\|_2]$, due to the use of a learned subgraph?

To that end, we assume for all $l \in L$, $\|\mathbf{W}\|_2 \leq \alpha < 1$ where α is a constant. This is reasonable since each $\mathbf{W}^{(l)}$ is typically controlled during training using regularization techniques, e.g., weight decay. As input features in \mathbf{X} are bounded, we also assume that there exists a constant β such that $\forall l > 0$, $\|\mathbf{H}\|_2^{(l)} \leq \beta$. We also assume that σ is Lipschitz continuous with Lipschitz constant L_σ . We assume ReLU activation to simplify our analysis since ReLU has a Lipschitz constant $L_\sigma = 1$. Under these assumptions, we have the following theorem (proof in Appendix A.4).

Theorem 4.2 (Error in GCN encodings). *For sufficiently deep L -layer GCN, the error in node embeddings*

$$\mathbb{E}[\lim_{L \rightarrow \infty} \|\tilde{\mathbf{H}}^{(L)} - \mathbf{H}^{*(L)}\|_2] < \frac{\beta}{1 - \alpha} \sqrt{2k(1 - \sum_{j=1}^{|\mathcal{E}|} \frac{(p_j^* + \tilde{p}_j - \epsilon)^2}{4})}.$$

4.4 SGS-GNN Training and Additional Details

Alg. 2 outlines the pseudocode for training SGS-GNN. SGS-GNN starts with two precomputation steps: i) computing the degree-proportionate edge weight as a *prior* to enhance the learned distribution \tilde{p} (line 1), and ii) partitioning the input graph using METIS (Karypis, 1997) for batch processing (line 2). Towards computing the loss for every partition at each iteration, SGS-GNN executes Edge probability encoding, Learned distribution augmentation with

Algorithm 2 SGS-GNN Training

```

1: Input:  $\mathcal{G}(\mathcal{V}, \mathcal{E}, \mathbf{X})$ , sample %  $q$ , #layers  $L$ , METIS Parts  $n$ 
2:  $p_{\text{prior}}(u, v) \leftarrow \frac{1/d_u + 1/d_v}{\sum_{i,j \in \mathcal{E}} (1/d_i + 1/d_j)}$ 
3:  $\mathcal{G}_{\text{parts}} \leftarrow \{\mathcal{G}_1, \mathcal{G}_2, \dots, \mathcal{G}_n\} = \text{METIS}(\mathcal{G}(\mathcal{V}, \mathcal{E}, p_{\text{prior}}), n)$ 
4: for epoch in max_epochs do
5:   for  $\mathcal{G}_i(\mathcal{V}_i, \mathcal{E}_i, \mathbf{X}_i, p_{\text{prior}}^i) \in \mathcal{G}_{\text{parts}}$  do
6:      $\tilde{p}, \mathbf{w} \leftarrow \text{EdgeMLP}(\mathcal{E}_i, \mathbf{X}_i, L)$  /* Algorithm 1 */
7:      $\tilde{p}_a \leftarrow \lambda \tilde{p} + (1 - \lambda) p_{\text{prior}}^i$  /* Augmenting  $\tilde{p}$  with prior */
8:      $\tilde{\mathcal{E}}, \tilde{\mathbf{w}} \leftarrow \text{Sample}(\tilde{p}_a, \mathbf{w}, \lfloor \frac{q|\mathcal{E}|}{100} \rfloor)$  /* Module II */
9:      $\hat{\mathbf{Y}}, \tilde{\mathbf{H}} \leftarrow \text{GNN}_\theta(\tilde{\mathcal{E}}, \mathbf{X}_i, \tilde{\mathbf{w}})$  /* Module III */
10:    Compute  $\mathcal{L}_{\text{CE}}, \mathcal{L}_{\text{assor}}$ , and  $\mathcal{L}_{\text{cons}}$  using  $\hat{\mathbf{Y}}, \tilde{\mathbf{H}}$ 
11:     $\mathcal{L} \leftarrow \alpha_1 \cdot \mathcal{L}_{\text{CE}} + \alpha_2 \cdot \mathcal{L}_{\text{assor}} + \alpha_3 \cdot \mathcal{L}_{\text{cons}}$ 
12:    Backward Propagate through  $\mathcal{L}$ 
13:   end for
14: end for
    
```

a prior, Sparse subgraph sampling and node embedding via GNN. Finally, the loss is backpropagated, the update pathways of which have been illustrated in Figure 2 earlier.

Batch processing. We can use EdgeMLP from Alg. 1 to compute edge weights in large-scale graphs, but efficient batch processing on edges is necessary for stochastic training of GNNs so as to reduce the risk of getting stuck in local minima. It is crucial to select a batch of edges that have high locality, preferably from within a cluster, and we utilize METIS to achieve this. We could have made partitions small enough to fit GPUs and then applying GNN without any sparsification, similar to ClusterGCN (Chiang et al., 2019). However, certain edges, such as task-irrelevant edges, may negatively impact performance, particularly in heterophilic or noisy graphs. In such cases, a high-quality learned sparse subgraph performs better than full graph, as validated in our experiments (§5.1.1).

Augmenting \tilde{p} with prior. While \tilde{p} can be directly used to sample sparse subgraphs, the resulting subgraph may be suboptimal for message passing due to missing bridge edges connecting low-degree node pairs. Thus augmenting the sampler with p_{prior} , which favors such edges, results in better quality sparse subgraph. p_{prior} is defined as

$$p_{\text{prior}}(u, v) \triangleq \frac{1/d_u + 1/d_v}{\sum_{i,j \in \mathcal{E}} (1/d_i + 1/d_j)}, \quad (16)$$

where d_u, d_v are degrees of nodes u, v . We control the emphasis of prior on the learned distribution with a parameter $\lambda \in [0, 1]$, resulting in the *augmented probability distribution*: $\tilde{p}_a(u, v) = \lambda \tilde{p}(u, v) + (1 - \lambda) p_{\text{prior}}(u, v)$ (line 7). The impact of p_{prior} on SGS-GNN is discussed in Appendix F.2.

Another enhancement we consider is the **conditional updates** to EdgeMLP. Since backpropagation is computationally expensive, we only update EdgeMLP when the training F1-score from the learned sparse subgraph exceeds the baseline subgraph from p_{prior} . The detailed algorithm for SGS-GNN with conditional updates is in Appendix C.

During inference, we use the learned probability distribution

from EdgeMLP, sample an ensemble of sparse subgraphs, and mean-aggregate their representations to produce final prediction on a test node. The pseudocode for inference (Alg. 4) is in Appendix C.

Computational Complexity. Suppose the number of hidden dimension $H \approx F$, where F is the dimension of the node features. The cost of an L -layer GCN is $\mathcal{O}(L(|\mathcal{E}| \cdot H + |\mathcal{V}| \cdot H^2))$ (Chiang et al., 2019). The cost of Alg 1 is $\mathcal{O}(L(|\mathcal{E}_{\text{sp}}| \cdot H + |\mathcal{V}| \cdot H^2) + |\mathcal{E}| \cdot H^2)$, since computing node-embedding (line 4, Alg. 1) using sparse graph \mathcal{E}_{sp} costs $\mathcal{O}(L(|\mathcal{E}_{\text{sp}}| \cdot H + |\mathcal{V}| \cdot H^2))$, and edge weight computation using MLP (line 5, Alg. 1) costs $\mathcal{O}(|\mathcal{E}| \cdot H^2)$. With an L -layer GCN used as downstream GNN acting on the sparse subgraph $\tilde{\mathcal{E}}$, the downstream GNN costs $\mathcal{O}(L(|\tilde{\mathcal{E}}| \cdot H + |\mathcal{V}| \cdot H^2))$. Since, $|\mathcal{E}_{\text{sp}}| = |\tilde{\mathcal{E}}|$ the total complexity of SGS-GNN (Alg. 2) is $\mathcal{O}(L(|\tilde{\mathcal{E}}| \cdot H + |\mathcal{V}| \cdot H^2) + |\mathcal{E}| \cdot H^2)$.

Space complexity. Let n partitions from METIS have similar sizes. The memory requirement for SGS-GNN with L -layer GCN is $\mathcal{O}\left(\frac{|\mathcal{E}| + |\mathcal{V}| \cdot H}{n} + L \cdot H^2\right)$.

5 Experiments

We experimented with 21 heterophilic and 12 homophilic benchmark datasets of varying sizes and homophily. Details about the datasets are provided in Appendix D. All experiments are carried out 10 times on a 24GB NVIDIA A10 Tensor Core GPU with 500GB internal memory, and with a data split of 20%/40%/40% (train/validation/test) unless specified otherwise. For baseline models, we follow the settings set by respective authors. We use 2 message passing layers for SGS-GNN and a hidden layer dimension of $H = 256$ for both EdgeMLP $_{\phi}$ and GNN $_{\theta}$. We set a dropout rate of 0.2 and use the Adam optimizer with a learning rate of 0.001. We trained all models for a maximum epoch of 500 with early stopping. The edge batch size is 500K, and the number of partitions for METIS is $n = \lceil |\mathcal{E}|/500K \rceil$. The percentage of edge sample is set to $q = 20\%$ following DropEdge (Rong et al., 2019). We take 10 samples of sparse subgraphs during inference. The model with the best validation F1-score is selected for testing. Our source codes are anonymously provided on Github¹.

Baselines. We use ClusterGCN (Chiang et al., 2019) to evaluate performance on the original large graphs. DropEdge (Rong et al., 2019), and GraphSAINT (GSAINT-E) (Zeng et al., 2019) are used as fixed distribution samplers. For Mixture of Graph (MOG) (Zhang et al., 2024), we use 3 experts and their recommended settings. We adjust the neighborhood sample size of NeuralSparse (Zheng et al., 2020) to have a similar sparsity as ours for a fair comparison.

¹<https://github.com/anonymousauthors001/SGS-GNN/>

Table 1: Mean F1-scores (in %) \pm std. dev. of various fixed distribution samplers using 20% edges. **Bold** indicates best-performing sampler excluding *Org. graph*.

DATASET	ORG. GRAPH	RANDOM	EDGE	ER	SGS-GNN
CORNELL	43.78 \pm 4.32	49.19 \pm 4.65	46.49 \pm 2.65	43.78 \pm 3.97	74.59 \pm 1.32
TEXAS	61.62 \pm 1.08	55.14 \pm 5.01	69.19 \pm 2.76	61.08 \pm 2.76	76.22 \pm 2.02
WISCONSIN	51.76 \pm 5.49	61.96 \pm 4.40	66.27 \pm 2.29	58.82 \pm 2.15	76.08 \pm 3.14
REED98	61.35 \pm 0.84	54.92 \pm 2.64	54.51 \pm 1.98	59.69 \pm 2.03	64.15 \pm 2.28
AMHERST41	61.83 \pm 0.30	57.49 \pm 0.81	57.40 \pm 0.58	50.60 \pm 1.14	72.75 \pm 0.59
PENN94	73.23 \pm 0.05	68.52 \pm 0.34	68.35 \pm 0.36	70.74 \pm 0.39	75.65 \pm 0.41
ROMAN-EMPIRE	44.25 \pm 0.16	43.08 \pm 0.61	42.91 \pm 0.63	58.18 \pm 1.25	64.69 \pm 0.12
CORNELL5	65.13 \pm 0.31	63.36 \pm 0.50	63.47 \pm 0.46	63.89 \pm 0.35	69.15 \pm 0.33
SQUIRREL	48.38 \pm 0.65	42.40 \pm 0.96	42.44 \pm 1.10	43.86 \pm 0.42	52.35 \pm 0.35
JOHNSHOPKINS55	68.71 \pm 0.28	63.40 \pm 0.53	62.80 \pm 0.74	62.14 \pm 2.51	73.80 \pm 0.33
ACTOR	28.42 \pm 0.23	32.37 \pm 0.78	30.53 \pm 0.59	32.03 \pm 0.27	33.88 \pm 0.42
MINESWEEPER	79.56 \pm 0.03	79.73 \pm 0.12	79.84 \pm 0.06	80.02 \pm 0.03	80.00 \pm 0.00
QUESTIONS	97.05 \pm 0.01	97.07 \pm 0.03	97.08 \pm 0.01	97.02 \pm 0.00	97.05 \pm 0.01
CHAMELEON	64.43 \pm 0.43	57.98 \pm 1.39	57.11 \pm 1.22	59.78 \pm 0.85	62.37 \pm 0.98
TOLOKERS	79.03 \pm 0.15	78.59 \pm 0.16	78.59 \pm 0.21	78.10 \pm 0.06	79.98 \pm 0.17
AMAZON-RATINGS	46.72 \pm 0.20	45.70 \pm 0.20	45.75 \pm 0.35	44.39 \pm 0.12	50.15 \pm 0.34
GENIUS	80.80 \pm 0.02	81.99 \pm 0.09	81.60 \pm 0.03	82.25 \pm 0.86	82.59 \pm 0.00
POKEC	62.05 \pm 0.37	60.30 \pm 0.27	60.17 \pm 0.17	58.76 \pm 0.59	60.49 \pm 0.10
ARXIV-YEAR	39.05 \pm 0.08	36.96 \pm 0.01	37.06 \pm 0.04	36.62 \pm 0.33	38.42 \pm 0.10
SNAP-PATENTS	35.38 \pm 0.15	34.57 \pm 0.08	34.48 \pm 0.16	33.13 \pm 0.37	35.41 \pm 0.10
OGBN-PROTEINS	93.15 \pm 0.00	93.15 \pm 0.00	93.15 \pm 0.00	93.15 \pm 0.00	93.15 \pm 0.00
CORA	67.29 \pm 0.51	61.20 \pm 7.76	57.63 \pm 14.73	66.90 \pm 0.17	65.58 \pm 0.69
DBLP	83.92 \pm 0.04	81.00 \pm 0.27	81.19 \pm 0.33	81.81 \pm 0.10	80.37 \pm 0.16
COMPUTERS	90.19 \pm 0.18	90.34 \pm 0.29	90.37 \pm 0.25	89.87 \pm 0.96	90.97 \pm 0.31
PUBMED	86.73 \pm 0.07	87.58 \pm 0.22	87.62 \pm 0.14	87.70 \pm 0.11	87.52 \pm 0.15
CORA_ML	86.29 \pm 0.51	85.39 \pm 0.35	85.29 \pm 0.60	85.63 \pm 0.51	83.99 \pm 0.53
SMALLCORA	80.28 \pm 0.37	75.82 \pm 0.54	76.44 \pm 1.21	75.90 \pm 1.25	76.94 \pm 0.76
CS	92.79 \pm 0.10	94.07 \pm 0.14	94.09 \pm 0.09	93.77 \pm 0.17	94.25 \pm 0.15
PHOTO	92.41 \pm 2.01	93.54 \pm 0.14	93.63 \pm 0.25	93.42 \pm 0.10	93.99 \pm 0.25
PHYSICS	96.08 \pm 0.03	96.20 \pm 0.07	96.23 \pm 0.12	96.22 \pm 0.07	96.27 \pm 0.09
CITESEER	91.44 \pm 0.29	86.38 \pm 0.26	86.75 \pm 0.22	86.24 \pm 0.26	86.78 \pm 0.28
WIKI	80.07 \pm 0.21	80.10 \pm 0.13	80.19 \pm 0.16	80.32 \pm 0.13	81.49 \pm 0.31
REDDIT	91.43 \pm 0.07	91.39 \pm 0.06	91.35 \pm 0.08	91.00 \pm 0.06	91.45 \pm 0.06
GEOM. MEAN	67.30	66.01	66.20	66.51	71.55

Additionally, we included SparseGAT (Ye & Ji, 2021) as another supervised method for generating sparse graphs.

5.1 Key Findings

In this section, we discuss the key findings supporting SGS-GNN. Empirical evaluation of various design choices in SGS-GNN and sensitivity of SGS-GNN to different values of hyperparameters are presented in Appendix F.

5.1.1 SGS-GNN VS. FIXED DISTR. SPARSIFIERS

We compare SGS-GNN with fixed edge distribution sparsifiers like *Random* from DropEdge, *Edge* sampler from GraphSAINT, and *Effective resistance (ER)*. Table 1 presents F1-scores, with the last row summarizing overall performance. The *Org. Graph* represents the original dense graph’s performance computed using ClusterGCN. Our learnable sampler EdgeMLP significantly outperforms fixed distribution samplers and original dense graphs in heterophilic datasets. In homophilic graphs, we observe a smaller margin of improvement, but SGS-GNN still outperforms other baselines.

5.1.2 SGS-GNN VS OTHER GNN BASED SPARSIFIERS

Table 2 compares SGS-GNN with related sparsification-based GNNs. We use GCN as the GNN module in our SGS-GNN. SGS-GNN significantly outperforms competing methods with a geometric mean improvement of 4 – 5% with only 20% of edges. Under similar settings, SGS-GNN significantly outperforms in heterophilic graphs and remains

Table 2: Mean F1-scores (in %) \pm std. dev. of baseline sparsifiers using 20% edges. **Bold** = best-performing method. OOM = out of memory. The geometric mean is computed across that dataset where all methods have results.

DATASET	GSAINT-E	DROPEDGE	MOG	SPARSEGAT	NEURALSPARSE	SGS-GNN
CORNELL	46.49 \pm 2.65	43.24 \pm 2.20	42.16 \pm 3.08	51.35 \pm 0.10	72.43 \pm 6.48	74.59 \pm 1.32
TEXAS	69.19 \pm 2.76	54.95 \pm 3.37	57.30 \pm 4.83	66.66 \pm 1.27	84.44 \pm 1.53	76.22 \pm 2.02
WISCONSIN	66.27 \pm 2.29	48.36 \pm 0.92	53.33 \pm 1.64	56.86 \pm 0.00	52.83 \pm 47.00	76.08 \pm 3.14
REED98	54.51 \pm 1.98	60.03 \pm 0.05	55.75 \pm 2.61	55.69 \pm 0.25	58.54 \pm 1.60	64.15 \pm 2.28
AMHERST41	57.40 \pm 0.58	59.00 \pm 18.80	56.78 \pm 2.05	49.00 \pm 0.20	56.85 \pm 75.00	72.75 \pm 0.59
PENNS94	68.35 \pm 0.36	65.87 \pm 0.30	OOM	65.00 \pm 0.10	OOM	75.65 \pm 0.31
ROMAN-EMPIRE	42.91 \pm 0.63	46.00 \pm 1.20	39.27 \pm 0.60	41.18 \pm 0.07	44.91 \pm 5.79	64.69 \pm 0.12
CORNELLS	63.47 \pm 0.46	61.40 \pm 1.45	OOM	53.77 \pm 0.39	OOM	69.15 \pm 0.43
Squirrel	42.44 \pm 1.10	48.60 \pm 0.00	27.67 \pm 0.51	29.50 \pm 0.00	38.24 \pm 0.00	52.35 \pm 0.35
JOHNSHOPKINS55	62.80 \pm 0.74	64.14 \pm 1.75	OOM	57.57 \pm 0.29	57.56 \pm 1.06	73.80 \pm 0.33
ACTOR	30.53 \pm 0.59	34.64 \pm 1.40	27.74 \pm 0.96	25.05 \pm 0.60	27.85 \pm 0.19	33.88 \pm 0.42
Minesweeper	79.84 \pm 0.06	80.00 \pm 0.00	80.00 \pm 0.00	80.00 \pm 0.00	80.00 \pm 0.10	80.00 \pm 0.00
QUESTIONS	97.08 \pm 0.01	97.00 \pm 0.01	97.04 \pm 0.01	97.08 \pm 0.01	97.02 \pm 0.01	97.05 \pm 0.01
Chameleon	57.11 \pm 1.22	50.60 \pm 0.04	53.25 \pm 0.63	60.60 \pm 0.15	60.52 \pm 0.78	62.37 \pm 0.98
TOLOKERS	78.59 \pm 0.21	78.40 \pm 0.20	78.49 \pm 0.28	78.20 \pm 0.72	78.16 \pm 0.00	79.98 \pm 0.17
AMAZON-RATINGS	45.75 \pm 0.35	43.87 \pm 0.67	41.18 \pm 0.49	44.23 \pm 0.05	47.05 \pm 0.47	50.15 \pm 0.34
CORA	57.63 \pm 14.73	65.09 \pm 0.44	67.26 \pm 1.11	61.07 \pm 0.39	56.68 \pm 0.32	65.58 \pm 0.69
DBLP	81.19 \pm 0.33	87.20 \pm 0.15	72.37 \pm 0.63	84.68 \pm 1.00	73.39 \pm 0.67	80.37 \pm 0.16
COMPUTERS	90.37 \pm 0.25	60.65 \pm 4.66	OOM	88.91 \pm 0.00	75.32 \pm 4.11	90.97 \pm 0.31
PUBMED	87.62 \pm 0.14	86.00 \pm 1.21	83.84 \pm 0.58	75.30 \pm 0.35	73.97 \pm 0.40	87.52 \pm 0.15
CORA_ML	85.29 \pm 0.60	84.80 \pm 0.20	OOM	80.60 \pm 0.40	79.30 \pm 0.87	83.99 \pm 0.53
SMALLCORA	76.44 \pm 1.21	76.47 \pm 0.31	78.43 \pm 0.73	75.70 \pm 0.43	75.79 \pm 9.00	76.94 \pm 0.76
CS	94.09 \pm 0.09	93.30 \pm 0.32	72.88 \pm 0.32	92.35 \pm 0.06	94.36 \pm 0.40	94.25 \pm 0.15
PHOTO	93.63 \pm 0.25	80.47 \pm 59.10	83.84 \pm 0.58	95.30 \pm 0.02	94.16 \pm 0.25	93.99 \pm 0.25
PHYSICS	96.23 \pm 0.12	97.28 \pm 0.70	OOM	95.96 \pm 0.06	96.38 \pm 0.04	96.27 \pm 0.09
CITESEER	86.75 \pm 0.22	77.40 \pm 0.10	78.43 \pm 0.73	58.75 \pm 0.10	65.40 \pm 1.20	86.78 \pm 0.28
WIKI	80.19 \pm 0.16	80.19 \pm 0.16	72.88 \pm 0.32	79.26 \pm 0.11	73.03 \pm 1.10	81.49 \pm 0.31
GEOM. MEAN*	64.88	63.58	59.49	61.07	64.10	71.93

competitive in homophilic graphs. We do not include results with large-scale graphs here since MOG and NeuralSparse goes out of memory in our computing environment. However, SGS-GNN can handle large graphs and the corresponding results are provided in Table 1.

5.1.3 SPARSITY VS. ACCURACY VS. HOMOPHILY

We analyzed the performance of SGS-GNN across varying homophily levels using synthetic and benchmark graphs in Fig. 3. Synthetic graphs were generated with node homophily \mathcal{H}_n at degree d by connecting $\lceil d\mathcal{H}_n \rceil$ edges to same-type neighbors and $d - \lceil d\mathcal{H}_n \rceil$ edges randomly. Results in Fig. 3(a) show that high homophily yields good performance regardless of sparsity, while high sparsity benefits heterophily, with optimal performance seen at 30% - 40% edge retention for heterophily levels 0.3 - 0.4. Furthermore, Fig. 3(b) indicates that while more edges improves accuracy on homophilic graphs, high sparsity can be advantageous on heterophilic graphs such as reed98 and amherst41, where we observe best performance at $\sim 20\%$ sparsity.

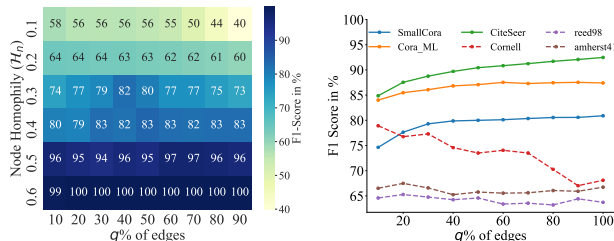


Figure 3: (Left) Heatmap of F1 scores (in %) at different homophily and sparsity levels (q) in Cora synthetic graphs. (Right) F1-scores of SGS-GNN at different sparsity for homophilic (solid line) and heterophilic (dashed line) graphs.

Fig. 4 shows that the sampled subgraph of SGS-GNN has a higher edge homophily than those by the fixed distribution

sparsifiers. This is expected due to our $\mathcal{L}_{\text{assor}}$ regularizer.

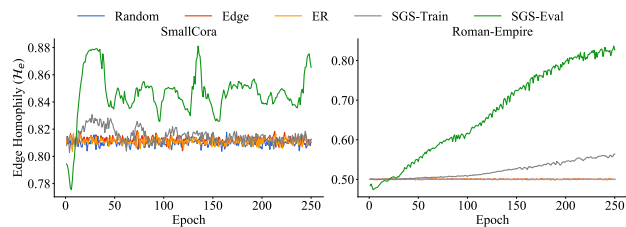


Figure 4: Edge homophily of selected subgraphs from different fixed distribution samplers vs. subgraphs from training and evaluation phase of SGS-GNN.

5.1.4 CONVERGENCE

To compare the sparsifiers in terms of convergence, we terminate training when the std. dev of loss in five consecutive epochs is $\leq 1e^{-3}$. Fig. 5 shows the bar plot of the number of epochs required for the methods to converge. SGS-GNN requires fewer iterations than other fixed distribution sparsifiers highlighting the benefit of learning the distribution.

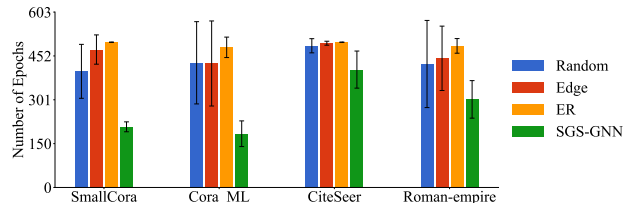


Figure 5: Number of epochs required by SGS-GNN to converge compared to other samplers under the same settings.

5.1.5 EFFICIENCY

Fig. 6 compares the training times per epoch of SGS-GNN with other GNN based sparsifier baselines. Under similar conditions, SGS-GNN is more efficient than NeuralSparse, MOG, and competitive with SparseGAT. SparseGAT is an implicit sparsifier; thus, unlike SGS-GNN, it is not memory efficient and cannot handle large graphs. Unsupervised sparsifiers such as DropEdge and GraphSAINT are more efficient but not always as effective as SGS-GNN (c.f. Tab. 2).

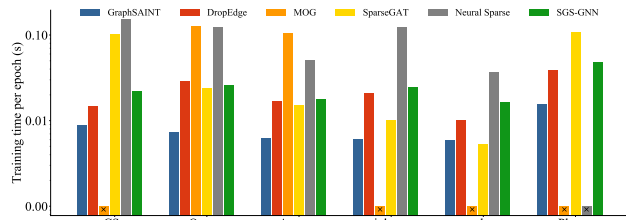


Figure 6: The bar shows the mean training time (s) per epoch (log scale) of SGS-GNN and related methods. The \times in the bar indicates out of memory. Under similar conditions, SGS-GNN is faster than NeuralSparse and MOG and competitive with SparseGAT.

6 Conclusion

We proposed SGS-GNN, a supervised graph sparsifier that produces a sparse subgraph with user-prescribed sparsity facilitating GNNs on large-scale graphs. We provided a theoretical analysis of SGS-GNN in terms of the quality of embedding it produces compared to an idealized, oracle sparsifier. Finally, we empirically validated the effectiveness, efficiency, and convergence of SGS-GNN over several baselines across homophilic and heterophilic graphs of various sizes. In the future, we plan to explore robustness aspect of our sparsifier in defense against adversarial noise.

Impact Statement

This paper presents a scalable supervised graph sparsification method that aims to support large-scale graph machine learning for Graph Neural Networks (GNNs). There are many potential societal consequences of our work. Positive consequences include making AI more accessible to smaller organizations and researchers with limited resources, as well as reducing the carbon footprint of AI models.

Acknowledgement

This work was supported in part by the U.S. Department of Energy, Office of Science, Office of Advanced Scientific Computing Research (ASCR) grant SC-0022260 and Computer Science Competitive Portfolios program at Pacific Northwest National Laboratory (PNNL); and by the Laboratory Directed Research and Development Program at PNNL. PNNL is a multi-program national laboratory operated for the U.S. Department of Energy (DOE) by Battelle Memorial Institute under Contract No. DE-AC05-76RL01830.

References

- Augustine, M. T. A survey on universal approximation theorems. *arXiv preprint arXiv:2407.12895*, 2024.
- Batson, J., Spielman, D. A., Srivastava, N., and Teng, S.-H. Spectral sparsification of graphs: theory and algorithms. *Communications of the ACM*, 56(8):87–94, 2013.
- Chen, H., Xu, Y., Huang, F., Deng, Z., Huang, W., Wang, S., He, P., and Li, Z. Label-aware graph convolutional networks. In *Proceedings of the 29th ACM International Conference on Information & Knowledge Management*, pp. 1977–1980, 2020.
- Chen, Y., Ye, H., Vedula, S., Bronstein, A., Dreslinski, R., Mudge, T., and Talati, N. Demystifying graph sparsification algorithms in graph properties preservation. *Proceedings of the VLDB Endowment*, 17(3):427–440, 2023.
- Chiang, W.-L., Liu, X., Si, S., Li, Y., Bengio, S., and Hsieh, C.-J. Cluster-GCN: An efficient algorithm for training deep and large graph convolutional networks. In *Proceedings of the 25th ACM SIGKDD International Conference on Knowledge Discovery & Data Mining*, pp. 257–266, 2019.
- Cybenko, G. Approximation by superpositions of a sigmoidal function. *Mathematics of control, signals and systems*, 2(4):303–314, 1989.
- Das, S. S., Ferdous, S., Halappanavar, M. M., Serra, E., and Pothen, A. AGS-GNN: Attribute-guided sampling for graph neural networks. In *Proceedings of the 30th ACM SIGKDD Conference on Knowledge Discovery and Data Mining*, pp. 538–549, 2024.
- Dragan, F. F., Fomin, F. V., and Golovach, P. A. Spanners in sparse graphs. *Journal of Computer and System Sciences*, 77(6):1108–1119, 2011.
- Fu, X., Zhang, J., Meng, Z., and King, I. Magnn: Metapath aggregated graph neural network for heterogeneous graph embedding. In *Proceedings of The Web Conference 2020*, pp. 2331–2341, 2020.
- Giles, C. L., Bollacker, K. D., and Lawrence, S. Citeseer: An automatic citation indexing system. In *Proceedings of the third ACM Conference on Digital Libraries*, pp. 89–98, 1998.
- Hamann, M., Lindner, G., Meyerhenke, H., Staudt, C. L., and Wagner, D. Structure-preserving sparsification methods for social networks. *Social Network Analysis and Mining*, 6:1–22, 2016.
- Hamilton, W., Ying, Z., and Leskovec, J. Inductive representation learning on large graphs. In *Advances in Neural Information Processing Systems*, pp. 1024–1034, 2017.
- Hashemi, M., Gong, S., Ni, J., Fan, W., Prakash, B. A., and Jin, W. A comprehensive survey on graph reduction: Sparsification, coarsening, and condensation. *arXiv:2402.03358*, 2024.
- He, M., Wei, Z., and Wen, J.-R. Convolutional neural networks on graphs with chebyshev approximation, revisited. *Advances in Neural Information Processing Systems*, 35: 7264–7276, 2022.
- Jang, E., Gu, S., and Poole, B. Categorical reparameterization with Gumbel-Softmax. *arXiv:1611.01144*, 2016.
- Jessica, L. S. E., Arafat, N. A., Lim, W. X., Chan, W. L., and Kong, A. W. K. Finite volume features, global geometry representations, and residual training for deep learning-based cfd simulation. In *Proceedings of the 41st International Conference on Machine Learning, ICML’24*. JMLR.org, 2024.

- Karypis, G. Metis: Unstructured graph partitioning and sparse matrix ordering system. *Technical report*, 1997.
- Kim, D. and Oh, A. How to find your friendly neighborhood: Graph attention design with self-supervision. *arXiv:2204.04879*, 2022.
- Kipf, T. N. and Welling, M. Semi-supervised classification with graph convolutional networks. *arXiv:1609.02907*, 2016.
- Leskovec, J., Kleinberg, J., and Faloutsos, C. Graph evolution: Densification and shrinking diameters. *ACM transactions on Knowledge Discovery from Data (TKDD)*, 1(1), 2007.
- Li, J., Zhang, T., Tian, H., Jin, S., Fardad, M., and Zafarani, R. Sgen: A graph sparsifier based on graph convolutional networks. In *Pacific-Asia Conference on Knowledge Discovery and Data Mining*, pp. 275–287. Springer, 2020.
- Lim, D., Hohne, F., Li, X., Huang, S. L., Gupta, V., Bhalerao, O., and Lim, S. N. Large scale learning on non-homophilous graphs: New benchmarks and strong simple methods. *Advances in Neural Information Processing Systems*, 34:20887–20902, 2021.
- Liu, Z., Zhou, K., Jiang, Z., Li, L., Chen, R., Choi, S.-H., and Hu, X. Dspar: An embarrassingly simple strategy for efficient gnn training and inference via degree-based sparsification. *Transactions on Machine Learning Research*, 2023.
- Luo, D., Cheng, W., Yu, W., Zong, B., Ni, J., Chen, H., and Zhang, X. Learning to drop: Robust graph neural network via topological denoising. In *Proceedings of the 14th ACM International Conference on Web Search and Data Mining*, pp. 779–787, 2021.
- Muzio, G., O’Bray, L., and Borgwardt, K. Biological network analysis with deep learning. *Briefings in bioinformatics*, 22(2):1515–1530, 2021.
- Namata, G., London, B., Getoor, L., Huang, B., and Edu, U. Query-driven active surveying for collective classification. In *10th International Workshop on Mining and Learning with Graphs*, volume 8, pp. 1, 2012.
- Pei, H., Wei, B., Chang, K. C.-C., Lei, Y., and Yang, B. Geom-GCN: Geometric graph convolutional networks. *arXiv:2002.05287*, 2020.
- Platonov, O., Kuznedelev, D., Babenko, A., and Prokhorenkova, L. Characterizing graph datasets for node classification: Beyond homophily-heterophily dichotomy. *arXiv:2209.06177*, 2022.
- Platonov, O., Kuznedelev, D., Diskin, M., Babenko, A., and Prokhorenkova, L. A critical look at the evaluation of gnn’s under heterophily: Are we really making progress? *arXiv:2302.11640*, 2023.
- Rong, Y., Huang, W., Xu, T., and Huang, J. Dropedge: Towards deep graph convolutional networks on node classification. *arXiv:1907.10903*, 2019.
- Rozemberczki, B., Allen, C., and Sarkar, R. Multi-scale attributed node embedding. *Journal of Complex Networks*, 9(2):cnab014, 2021.
- Sen, P., Namata, G., Bilgic, M., Getoor, L., Galligher, B., and Eliassi-Rad, T. Collective classification in network data. *AI magazine*, 29(3):93–93, 2008.
- Shchur, O., Mumme, M., Bojchevski, A., and Günnemann, S. Pitfalls of graph neural network evaluation. *arXiv:1811.05868*, 2018.
- Spielman, D. A. and Srivastava, N. Graph sparsification by effective resistances. *SIAM Journal on Computing*, 40(6):1913–1926, 2011.
- Srinivasa, R. S., Xiao, C., Glass, L., Romberg, J., and Sun, J. Fast graph attention networks using effective resistance based graph sparsification. *arXiv:2006.08796*, 2020.
- Su, Z., Liu, Y., Kurths, J., and Meyerhenke, H. Generic network sparsification via degree- and subgraph-based edge sampling. *Information Sciences*, 679:121096, 2024.
- Veličković, P., Cucurull, G., Casanova, A., Romero, A., Lio, P., and Bengio, Y. Graph attention networks. *arXiv:1710.10903*, 2017.
- Voudigari, E., Salamanos, N., Papageorgiou, T., and Yannakoudakis, E. J. Rank degree: An efficient algorithm for graph sampling. In *International Conference on Advances in Social Networks Analysis and Mining (ASONAM)*, pp. 120–129. IEEE, 2016.
- Wang, Z., He, Y., and Liu, B. Probability passing for graph neural networks: Graph structure and representations joint learning. *arXiv:2407.10688*, 2024.
- Wu, G., Lin, S., Zhuang, Y., and Qiao, J. Alleviating over-smoothing via graph sparsification based on vertex feature similarity. *Applied Intelligence*, 53(17):20223–20238, 2023.
- Wu, J., Wang, X., Feng, F., He, X., Chen, L., Lian, J., and Xie, X. Self-supervised graph learning for recommendation. In *Proceedings of the 44th international ACM SIGIR conference on research and development in information retrieval*, pp. 726–735, 2021.

- Wu, L., Cui, P., Pei, J., and Zhao, L. *Graph Neural Networks: Foundations, Frontiers, and Applications*. Springer Singapore, Singapore, 2022.
- Xie, R. *Distributionally Robust Optimization and its Applications in Power System Energy Storage Sizing*. Springer Nature, 2024.
- Xu, K., Hu, W., Leskovec, J., and Jegelka, S. How powerful are graph neural networks? *arXiv:1810.00826*, 2018.
- Xu, X., Yuruk, N., Feng, Z., and Schweiger, T. A. SCAN: A structural clustering algorithm for networks. In *Proceedings of the 13th ACM SIGKDD international conference on knowledge discovery and data mining*, pp. 824–833, 2007.
- Ye, Y. and Ji, S. Sparse graph attention networks. *IEEE Transactions on Knowledge and Data Engineering*, 35(1):905–916, 2021.
- Yu, J., Yin, H., Xia, X., Chen, T., Cui, L., and Nguyen, Q. V. H. Are graph augmentations necessary? simple graph contrastive learning for recommendation. In *Proceedings of the 45th international ACM SIGIR conference on research and development in information retrieval*, pp. 1294–1303, 2022.
- Zeng, H., Zhou, H., Srivastava, A., Kannan, R., and Prasanna, V. GraphSAINT: Graph sampling based inductive learning method. In *International Conference on Learning Representations*, 2019.
- Zhang, G., Sun, X., Yue, Y., Jiang, C., Wang, K., Chen, T., and Pan, S. Graph Sparsification via Mixture of Graphs. *arXiv:2405.14260*, 2024.
- Zheng, C., Zong, B., Cheng, W., Song, D., Ni, J., Yu, W., Chen, H., and Wang, W. Robust graph representation learning via neural sparsification. In *International Conference on Machine Learning*, pp. 11458–11468. PMLR, 2020.
- Zhou, J., Cui, G., Hu, S., Zhang, Z., Yang, C., Liu, Z., Wang, L., Li, C., and Sun, M. Graph neural networks: A review of methods and applications. *AI open*, 1:57–81, 2020.
- Zhu, J., Yan, Y., Zhao, L., Heimann, M., Akoglu, L., and Koutra, D. Beyond homophily in graph neural networks: Current limitations and effective designs. *Advances in Neural Information Processing Systems*, 33:7793–7804, 2020.

A Theoretical Analysis

A.1 Notations

We dedicate Table 3 to index the notations used in this paper. Note that every notation is also defined when it is introduced.

Table 3: Notations.

\mathcal{G}	\triangleq	Input graph with a vertex set \mathcal{V} , an edge set \mathcal{E} , and features \mathbf{X}
\mathbf{A}	\triangleq	Adjacency matrix of \mathcal{G}
\mathcal{E}	\triangleq	Edges of \mathcal{G}
\mathcal{V}	\triangleq	Nodes of \mathcal{G}
\mathbf{X}	\triangleq	Matrix containing node features of \mathcal{G}
\mathbf{y}	\triangleq	Vector of node labels of \mathcal{G}
C	\triangleq	An ordered set containing all possible node labels of \mathcal{G}
F	\triangleq	Dimension of node features in \mathcal{G}
L	\triangleq	Number of GNN layers
H	\triangleq	Node embedding dimension
\mathbf{H}	\triangleq	Node embedding matrix
h_u	\triangleq	Embedding of node u
\mathbf{w}	\triangleq	Vector of edge weights in \mathcal{G}
q	\triangleq	Ratio of # edges in sparse graph and # edges in input graph in %
k	\triangleq	# edges in the sparse graph, $k \triangleq \lfloor \frac{q \mathcal{E} }{100} \rfloor$
\tilde{p}	\triangleq	Learned probability distribution by SGS-GNN
$\tilde{\mathcal{E}}$	\triangleq	Set of edges sampled from \mathcal{E} by SGS-GNN following \tilde{p}
$\tilde{\mathcal{G}}$	\triangleq	Sparse subgraph $(\mathcal{V}, \tilde{\mathcal{E}}, \mathbf{X})$ constructed by SGS-GNN
$\mathbf{A}_{\tilde{\mathcal{G}}}$ or $\tilde{\mathbf{A}}$	\triangleq	Adjacency matrix of $\tilde{\mathcal{G}}$
\tilde{w}	\triangleq	Edge weight of sparse graph learned by SGS-GNN
p_{prior}	\triangleq	Probability distribution of a fixed prior on \mathcal{G}
\tilde{p}_a	\triangleq	Augmented learned probability distribution
p^*	\triangleq	True probability distribution known by the idealized learning ORACLE
\mathcal{E}^*	\triangleq	Set of edges sampled from \mathcal{E} by the learning ORACLE following distribution p^*
\mathcal{G}^*	\triangleq	True sparse subgraph $(\mathcal{V}, \mathcal{E}^*, \mathbf{X})$ constructed by the learning ORACLE
$\mathbf{A}_{\mathcal{G}^*}$ or \mathbf{A}^*	\triangleq	Adjacency matrix of \mathcal{G}^*
\mathcal{L}_{CE}	\triangleq	Cross entropy loss
$\mathcal{L}_{\text{assort}}$	\triangleq	Assortative loss
$\mathcal{L}_{\text{cons}}$	\triangleq	Consistency loss
\mathcal{L}	\triangleq	Total loss

A.2 Bounding #common edges wrt. true subgraph

Let \mathcal{E}^* and $\tilde{\mathcal{E}}$ denote the ordered collection of edges sampled by the idealized learning ORACLE according to true distribution p^* and by SGS-GNN according to learned probability \tilde{p} respectively. For analytical convenience, let us assume that both learning algorithms sample $k = \lfloor q|\mathcal{E}|/100 \rfloor$ edges with replacement independently.

First, we will prove lemma A.1, which show that the probability of an edge chosen by SGS-GNN coincides with that chosen by the ORACLE has a lower bound. Finally, we will prove one of the main results (Theorem A.2), which shows that given $q \in [0, 100]$, we can lower-bound the expected number of common edges between SGS-GNN and the learning ORACLE.

Lemma A.1. *For any arbitrarily chosen $i \in \{1, 2, \dots, k\}$*

$$\Pr(\mathcal{E}_i^* = \tilde{\mathcal{E}}_i) \geq \sum_{j=1}^{|\mathcal{E}|} \frac{(p_j^* + \tilde{p}_j - \epsilon)^2}{4},$$

where $k = \lfloor q|\mathcal{E}|/100 \rfloor$ and $0 \leq q \leq 100$ is a user-specified parameter and $\epsilon \in [0, 1]$ is the error.

Proof. We prove the above lemma in two parts.

Part 1: Universal approximation of probability distribution over edges. The Universal Approximation Theorem (Cybenko, 1989; Augustine, 2024) states that a feed-forward neural network with at least one hidden layer and a finite number of neurons can approximate any continuous function $f : \mathbb{R}^n \rightarrow \mathbb{R}$ on a compact subset of \mathbb{R}^n , given a suitable choice of weights and activation functions.

In our case, $p^* = f$ is the true edge probability distribution for the downstream task, $\tilde{p} = f_{\text{MLP},\phi}$ is the learned approximate distribution and \mathbf{x}_e is a vector of edge features, for instance, $\mathbf{x}_e = ((\mathbf{h}_u - \mathbf{h}_v) \oplus (\mathbf{h}_u \odot \mathbf{h}_v))$ as used in equation 7. The following universal approximation property holds for the module I component of SGS-GNN,

$$\sup_{e \in \mathcal{E}} \|\tilde{p}(\mathbf{x}_e) - p^*(\mathbf{x}_e)\|_1 \leq \epsilon. \quad (17)$$

Here, we have two underlying assumptions: (i) the optimal distribution p^* is a function of node features \mathbf{X} and (ii) \mathbf{X} is a compact subset (bounded and closed) of Euclidean space \mathbb{R}^n . The first assumption is made to simplify the problem. The second assumption is quite practical since the node features are typically normalized. Hence, we can show that the embeddings $\mathbf{h}_u, \mathbf{h}_v$, which are continuous images of \mathbf{X} , are also compact due to the extreme value theorem. As a result, the edge features \mathbf{x}_e which, in a sense, *lifts* the end-point node features into higher-dimensional Euclidean space are also compact. The approximation error ϵ can be made arbitrarily small by increasing the capacity of the MLP, e.g., adding more neurons or layers.

Part 2: Common edges wrt. optimal subgraph. The event $\mathcal{E}_i^* = \tilde{\mathcal{E}}_i$ means that both \mathcal{E}_i^* and $\tilde{\mathcal{E}}_i$ contain the same edge. But there are $|\mathcal{E}|$ such candidates. Hence, the probability of this event is given by,

$$\begin{aligned} \Pr(\mathcal{E}_i^* = \tilde{\mathcal{E}}_i) &= \sum_{j=1}^{|\mathcal{E}|} \Pr(\mathcal{E}_i^* = \mathcal{E}_j \wedge \tilde{\mathcal{E}}_i = \mathcal{E}_j), \\ &= \sum_{j=1}^{|\mathcal{E}|} \Pr(\mathcal{E}_i^* = \mathcal{E}_j) \cdot \Pr(\tilde{\mathcal{E}}_i = \mathcal{E}_j), \\ &= \sum_{j=1}^{|\mathcal{E}|} p_j^* \cdot \tilde{p}_j, \\ &\geq \sum_{j=1}^{|\mathcal{E}|} \frac{(p_j^* + \tilde{p}_j - |p_j^* - \tilde{p}_j|)^2}{4}, \\ &\geq \sum_{j=1}^{|\mathcal{E}|} \frac{(p_j^* + \tilde{p}_j - \epsilon)^2}{4}. \end{aligned}$$

The second line follows since the optimal sampler is a different algorithm independent from the sampler used in SGS-GNN. The last line follows because $\|p_j^* - \tilde{p}_j\|_1 \leq \epsilon \implies |p_j^* - \tilde{p}_j| \leq \epsilon$ (from eq. 17). \square

We have the following theorem that lower-bounds the number of common edges with respect to the optimal sampler $|\mathcal{E}^* \cap \tilde{\mathcal{E}}|$:

Theorem A.2 (Lower-bound).

$$\mathbb{E}[|\mathcal{E}^* \cap \tilde{\mathcal{E}}|] \geq k \sum_{j=1}^{|\mathcal{E}|} \frac{(p_j^* + \tilde{p}_j - \epsilon)^2}{4}, \quad (18)$$

where $k = \lfloor q|\mathcal{E}|/100 \rfloor$ and $0 \leq q \leq 100$ is a user-specified parameter.

Proof. Since we are drawing k edges independently at random, the theorem follows by applying the linearity of expectation

on the following:

$$\begin{aligned}\mathbb{E}[|\mathcal{E}^* \cap \tilde{\mathcal{E}}|] &= \mathbb{E}\left[\sum_{i=1}^k \mathbb{I}(\mathcal{E}_i^* = \tilde{\mathcal{E}}_i)\right] = \sum_{i=1}^k \Pr(\mathcal{E}_i^* = \tilde{\mathcal{E}}_i) \\ &= k \cdot \Pr(\mathcal{E}_i^* = \tilde{\mathcal{E}}_i) \\ &\geq k \sum_{j=1}^{|\mathcal{E}|} \frac{(p_j^* + \tilde{p}_j - \epsilon)^2}{4}\end{aligned}$$

□

This theorem shows that the expected number of common edges between the sample subgraph obtained by SGS-GNN $\tilde{\mathcal{G}}$ and the true optimal sample subgraph \mathcal{G}^* is non-trivial.

Theorem A.3 (Upper-bound).

$$\mathbb{E}[|\mathcal{E}^* \cap \tilde{\mathcal{E}}|] \leq k\left(1 - \frac{\|p^* - \tilde{p}\|_1}{2}\right), \quad (19)$$

where $k = \lfloor q|\mathcal{E}|/100 \rfloor$ and $0 \leq q \leq 100$ is a user-specified parameter.

Proof.

$$\begin{aligned}\Pr(\mathcal{E}_i^* = \tilde{\mathcal{E}}_i) &= \sum_{j=1}^{|\mathcal{E}|} p_j^* \cdot \tilde{p}_j \\ &\leq \sum_{j=1}^{|\mathcal{E}|} \min(p_j^*, \tilde{p}_j) \\ &= 1 - d_{TV}(p^*, \tilde{p}) \\ &= 1 - \frac{1}{2}\|p^* - \tilde{p}\|_1\end{aligned}$$

□

Here d_{TV} is the total variation distance. The result used in the last line regarding d_{TV} can be found in Xie (2024).

The implication of the upper-bound. When $\tilde{p} \rightarrow p^*$, the norm $\|p^* - \tilde{p}\|_1 \rightarrow 0$; therefore, the number of common edges could be close to k .

A.3 Upper-bounding the error in the learned Adjacency matrix

With the bound proven earlier on the #common edges by the sparse subgraph of SGS-GNN with that by a learning ORACLE, in this section, we want to obtain an upper-bound on the error in terms of the norm of the Adjacency matrices. As adjacency matrices are used by GNNs for computing node embeddings, such result is important for obtaining error bound on the embeddings later on.

Let $\mathbf{A}_{\tilde{\mathcal{G}}}$ and $\mathbf{A}_{\mathcal{G}^*}$ be the corresponding adjacency matrices of the learned sparse graph $\tilde{\mathcal{G}}$ and true optimal sparse graph \mathcal{G}^* . The dimension of these matrices is the same as the input adjacency matrix $\mathbf{A}_{\mathcal{G}}$ except that $\mathbf{A}_{\mathcal{G}}$ is denser. Let us also denote the Frobenius norm of a matrix \mathbf{A} as $\|\mathbf{A}\|_F$ and the spectral norm of \mathbf{A} as $\|\mathbf{A}\|_2$. The Frobenius norm of \mathbf{A} is defined as $\sqrt{\sum_{ij} \mathbf{A}_{ij}^2}$, whereas the spectral norm of \mathbf{A} is the largest singular value $\sigma_{max}(\mathbf{A})$ of \mathbf{A} .

Since SGS-GNN do not know the true probability distribution p^* , error is introduced in the learned adjacency matrix $\mathbf{A}_{\tilde{\mathcal{G}}}$ of the downstream sparse subgraph. We are interested in analyzing the expected error introduced in $\mathbf{A}_{\tilde{\mathcal{G}}}$ in terms of the spectral norm, to be precise, $\mathbb{E}[\|\mathbf{A}_{\tilde{\mathcal{G}}} - \mathbf{A}_{\mathcal{G}^*}\|_2]$. To this end, we will exploit the lower bound derived in Theorem 1 and the fact that $\|\mathbf{A}\|_2 \leq \|\mathbf{A}\|_F$.

Lemma A.4 (Error in Adjacency matrix approximation). *Let $\mathbf{A}_{\tilde{\mathcal{G}}}$ and $\mathbf{A}_{\mathcal{G}^*}$ be the corresponding adjacency matrices of the learned sparse graph $\tilde{\mathcal{G}}$ and true optimal sparse graph \mathcal{G}^* . If the downstream sampler sampled k edges independently at random (with replacement) to construct those matrices following their respective distributions \tilde{p} and p^* , then*

$$\mathbb{E}[\|\mathbf{A}_{\tilde{\mathcal{G}}} - \mathbf{A}_{\mathcal{G}^*}\|_2] \leq \sqrt{2k\left(1 - \sum_{j=1}^{|\mathcal{E}|} \frac{(p_j^* + \tilde{p}_j - \epsilon)^2}{4}\right)},$$

where $k = \lfloor q|\mathcal{E}|/100 \rfloor$ and $0 \leq q \leq 100$ is a user-specified parameter.

Proof. Since the entries in adjacency matrices are either 0 or 1, the difference $\mathbf{A}_{\tilde{\mathcal{G}}}(i, j) - \mathbf{A}_{\mathcal{G}^*}(i, j)$ are in $\{-1, 0, 1\}$ for all i, j . The following holds by definition of Frobenius norm,

$$\|\mathbf{A}_{\tilde{\mathcal{G}}} - \mathbf{A}_{\mathcal{G}^*}\|_F^2 = \sum_{ij} (\mathbf{A}_{\tilde{\mathcal{G}}}(i, j) - \mathbf{A}_{\mathcal{G}^*}(i, j))^2.$$

As a result, only the non-zero entries in $\mathbf{A}_{\tilde{\mathcal{G}}} - \mathbf{A}_{\mathcal{G}^*}$ contribute to the square of Frobenius norm $\|\mathbf{A}_{\tilde{\mathcal{G}}} - \mathbf{A}_{\mathcal{G}^*}\|_F^2$. The expected number of non-zero entries in $\|\mathbf{A}_{\tilde{\mathcal{G}}} - \mathbf{A}_{\mathcal{G}^*}\|_F^2$ corresponds to the expected cardinality $|(\tilde{\mathcal{E}} \setminus \mathcal{E}^*) \cup (\mathcal{E}^* \setminus \tilde{\mathcal{E}})|$. Thus

$$\begin{aligned} \mathbb{E}[\|\mathbf{A}_{\tilde{\mathcal{G}}} - \mathbf{A}_{\mathcal{G}^*}\|_F^2] &= \mathbb{E}[|(\tilde{\mathcal{E}} \setminus \mathcal{E}^*) \cup (\mathcal{E}^* \setminus \tilde{\mathcal{E}})|] \\ &= \mathbb{E}[|\tilde{\mathcal{E}}| + |\mathcal{E}^*| - 2|\tilde{\mathcal{E}} \cap \mathcal{E}^*|] \\ &= 2k - 2\mathbb{E}[|\tilde{\mathcal{E}} \cap \mathcal{E}^*|] \\ &\leq 2k - 2k \sum_{j=1}^{|\mathcal{E}|} \frac{(p_j^* + \tilde{p}_j - \epsilon)^2}{4} \\ &= 2k\left(1 - \sum_{j=1}^{|\mathcal{E}|} \frac{(p_j^* + \tilde{p}_j - \epsilon)^2}{4}\right). \end{aligned}$$

Applying Jensen's inequality for convex functions, in particular, applying $(\mathbb{E}[\mathbf{X}])^2 \leq \mathbb{E}[\mathbf{X}^2]$ yields,

$$\begin{aligned} (\mathbb{E}[\|\mathbf{A}_{\tilde{\mathcal{G}}} - \mathbf{A}_{\mathcal{G}^*}\|_F])^2 &\leq \mathbb{E}[\|\mathbf{A}_{\tilde{\mathcal{G}}} - \mathbf{A}_{\mathcal{G}^*}\|_F^2] \\ &\leq 2k\left(1 - \sum_{j=1}^{|\mathcal{E}|} \frac{(p_j^* + \tilde{p}_j - \epsilon)^2}{4}\right). \end{aligned}$$

Taking square-root on both sides yields,

$$\mathbb{E}[\|\mathbf{A}_{\tilde{\mathcal{G}}} - \mathbf{A}_{\mathcal{G}^*}\|_F] \leq \sqrt{2k\left(1 - \sum_{j=1}^{|\mathcal{E}|} \frac{(p_j^* + \tilde{p}_j - \epsilon)^2}{4}\right)}.$$

We obtain the theorem using the following relation between the Frobenius and spectral norms.

$$\begin{aligned} \|\mathbf{A}_{\tilde{\mathcal{G}}} - \mathbf{A}_{\mathcal{G}^*}\|_2 &\leq \|\mathbf{A}_{\tilde{\mathcal{G}}} - \mathbf{A}_{\mathcal{G}^*}\|_F \\ \implies \mathbb{E}[\|\mathbf{A}_{\tilde{\mathcal{G}}} - \mathbf{A}_{\mathcal{G}^*}\|_2] &\leq \mathbb{E}[\|\mathbf{A}_{\tilde{\mathcal{G}}} - \mathbf{A}_{\mathcal{G}^*}\|_F] \\ &= \sqrt{2k\left(1 - \sum_{j=1}^{|\mathcal{E}|} \frac{(p_j^* + \tilde{p}_j - \epsilon)^2}{4}\right)} \end{aligned}$$

□

A.4 Upper-bounding the error in the predicted node embeddings

We consider vanilla GCN as proof of concept to understand how the changes in the sparse subgraph affect the node embeddings produced by a trained GCN. Our goal is to analyze the respective encodings produced by an L -layer GCN when the input subgraphs are \mathcal{G}^* (corresponding to $\mathbf{A}_{\mathcal{G}^*}$) and $\tilde{\mathcal{G}}$ (corresponding to $\mathbf{A}_{\tilde{\mathcal{G}}}$) respectively. For simplicity, we will shorten the matrices $\mathbf{A}_{\mathcal{G}^*}$ as \mathbf{A}^* and $\mathbf{A}_{\tilde{\mathcal{G}}}$ as $\hat{\mathbf{A}}$.

A single GCN layer is defined as,

$$\mathbf{H}^{(l+1)} = \sigma(\hat{\mathbf{A}}\mathbf{H}^{(l)}\mathbf{W}^{(l)}),$$

where $\hat{\mathbf{A}} = \mathbf{D}^{-1/2}\mathbf{A}\mathbf{D}^{-1/2}$ is the normalized adjacency matrix, $\mathbf{H}^{(l)}$ is the input to the l -th layer with $\mathbf{H}^{(0)} = \mathbf{X}$, $\mathbf{W}^{(l)}$ is the learnable weight matrix for l -th layer and σ is non-linear activation function. Let us suppose an L -layer GCN produces embeddings $\tilde{\mathbf{H}}^{(L)}$ and $\mathbf{H}^{*(L)}$ when it takes sparse matrices $\hat{\mathbf{A}}$ and \mathbf{A}^* as input. We want to upper-bound,

$$\mathbb{E}[\|\tilde{\mathbf{H}}^{(L)} - \mathbf{H}^{*(L)}\|_2],$$

in other words, the loss in the downstream node encodings is due to using our learned subgraph.

Assumptions. We assume that for all l , $\|\mathbf{W}^{(l)}\|_2 \leq \alpha < 1$ where α is a constant no more than 1. This is reasonable since each $\mathbf{W}^{(l)}$ is typically controlled during training using regularization techniques, e.g., weight decay. Assuming that the input features in \mathbf{X} are bounded, we can also assume that there exists a constant β such that $\forall l$, $\|\mathbf{H}^{(l)}\|_2 \leq \beta$. We also assume that σ is *Lipschitz continuous* with *Lipschitz constant* L_σ ; for instance, activation functions such as ReLU, sigmoid, or tanH are Lipschitz continuous. In particular, we assume ReLU activation for our theoretical analysis because ReLU has *Lipschitz constant* $L_\sigma = 1$, which simplifies our analysis.

Under these assumptions, we have the following theorem,

Theorem A.5 (Error in GCN encodings). *For sufficiently deep L -layer GCN (large L), the error*

$$\mathbb{E}[\lim_{L \rightarrow \infty} \|\tilde{\mathbf{H}}^{(L)} - \mathbf{H}^{*(L)}\|_2] < \frac{\beta}{1 - \alpha} \sqrt{2k(1 - \sum_{j=1}^{|\mathcal{E}|} \frac{(p_j^* + \tilde{p}_j - \epsilon)^2}{4})}.$$

Proof.

$$\tilde{\mathbf{H}}^{(L)} - \mathbf{H}^{*(L)} = \sigma(\hat{\mathbf{A}}\tilde{\mathbf{H}}^{(L-1)}\mathbf{W}^{(L-1)}) - \sigma(\hat{\mathbf{A}}^*\mathbf{H}^{*(L-1)}\mathbf{W}^{(L-1)})$$

Since σ is a Lipschitz continuous function, we have

$$\begin{aligned} \|\tilde{\mathbf{H}}^{(L)} - \mathbf{H}^{*(L)}\|_2 &\leq L_\sigma \|\hat{\mathbf{A}}\tilde{\mathbf{H}}^{(L-1)}\mathbf{W}^{(L-1)} - \hat{\mathbf{A}}^*\mathbf{H}^{*(L-1)}\mathbf{W}^{(L-1)}\|_2 \\ &= \|\hat{\mathbf{A}}\tilde{\mathbf{H}}^{(L-1)}\mathbf{W}^{(L-1)} - \hat{\mathbf{A}}^*\mathbf{H}^{*(L-1)}\mathbf{W}^{(L-1)}\|_2 \\ &= \|(\hat{\mathbf{A}} - \hat{\mathbf{A}}^*)\tilde{\mathbf{H}}^{(L-1)}\mathbf{W}^{(L-1)} + \hat{\mathbf{A}}^*(\tilde{\mathbf{H}}^{(L-1)} - \mathbf{H}^{*(L-1)})\mathbf{W}^{(L-1)}\|_2 \end{aligned}$$

For notational convenience, let us suppose $D^{(L)} = \|\tilde{\mathbf{H}}^{(L)} - \mathbf{H}^{*(L)}\|_2$. Applying the sub-multiplicative property of the spectral norm and triangle inequality, we obtain the following recurrence relation

$$\begin{aligned} D^{(L)} &\leq \|(\hat{\mathbf{A}} - \hat{\mathbf{A}}^*)\|_2 \|\tilde{\mathbf{H}}^{(L-1)}\|_2 \|\mathbf{W}^{(L-1)}\|_2 + \|\hat{\mathbf{A}}^*\|_2 D^{(L-1)} \|\mathbf{W}^{(L-1)}\|_2 \\ &\leq \|(\hat{\mathbf{A}} - \hat{\mathbf{A}}^*)\|_2 \beta \alpha + \|\hat{\mathbf{A}}^*\|_2 D^{(L-1)} \alpha \\ &\leq \|(\hat{\mathbf{A}} - \hat{\mathbf{A}}^*)\|_2 \beta \alpha + D^{(L-1)} \alpha \end{aligned}$$

The last inequality holds because normalized adjacency matrix satisfies $\|\hat{\mathbf{A}}^*\|_2 \leq 1$. This is because $\hat{\mathbf{A}}^*$ is symmetric, row-stochastic matrix. Thus the singular values of $\hat{\mathbf{A}}^*$ is the absolute values of eigenvalues of $\hat{\mathbf{A}}^*$ and the largest singular value of $\hat{\mathbf{A}}^*$ is the largest eigenvalue of $\hat{\mathbf{A}}^*$. But $\hat{\mathbf{A}}^*$ being row-stochastic, its largest eigenvalue is at most 1 hence $\|\hat{\mathbf{A}}^*\|_2 = \sigma_{max}(\hat{\mathbf{A}}^*) \leq 1$.

By unrolling the recursion from earlier inequality:

$$D^{(L)} \leq \|(\hat{\mathbf{A}} - \hat{\mathbf{A}}^*)\|_2 \beta \alpha \sum_{l=0}^{L-1} \alpha^l + D^{(0)} \alpha^L$$

$D^{(0)} = \|\tilde{\mathbf{H}}^{(0)} - \mathbf{H}^{*(0)}\|_2 = \|\mathbf{X} - \mathbf{X}\|_2 = 0$. Since $\alpha < 1$, The geometric series simplifies to:

$$\begin{aligned} \sum_{l=0}^{L-1} \alpha^l &= \frac{1 - \alpha^L}{1 - \alpha} \\ \lim_{L \rightarrow \infty} \sum_{l=0}^{L-1} \alpha^l &= \frac{1}{1 - \alpha} \end{aligned}$$

Thus our earlier inequality becomes:

$$\lim_{L \rightarrow \infty} D^{(L)} \leq \frac{\beta \alpha}{1 - \alpha} \|(\hat{\mathbf{A}} - \hat{\mathbf{A}}^*)\|_2 < \frac{\beta}{1 - \alpha} \|(\hat{\mathbf{A}} - \hat{\mathbf{A}}^*)\|_2$$

Taking expectation on both sides gives us our desired result:

$$\begin{aligned} \mathbb{E}[\lim_{L \rightarrow \infty} \|\tilde{\mathbf{H}}^{(L)} - \mathbf{H}^{*(L)}\|_2] &= \mathbb{E}[D^{(L)}] < \frac{\beta}{1 - \alpha} \mathbb{E}[\|(\hat{\mathbf{A}} - \hat{\mathbf{A}}^*)\|_2] \\ &< \frac{\beta}{1 - \alpha} \mathbb{E}[\|(\hat{\mathbf{A}} - \mathbf{A}^*)\|_2] \\ &= \frac{\beta}{1 - \alpha} \sqrt{2k(1 - \sum_{j=1}^{|\mathcal{E}|} \frac{(p_j^* + \tilde{p}_j - \epsilon)^2}{4})} \end{aligned}$$

□

B Analyzing the Effectiveness of SGS-GNN with a Synthetic Graph

In this section, we demonstrate and analyze the effectiveness of SGS-GNN with a synthetically generated heterophilic graph.

Synthetic Graph: Moon. The moon dataset has the following properties: number of nodes $|\mathcal{V}| = 150$, number of edges $|\mathcal{E}| = 870$, average degree $d = 5.8$, node homophily $\mathcal{H}_n = 0.2$, edge homophily $\mathcal{H}_e = 0.32$, training/test split = 30%/70%, and 2D coordinates of the points representing the nodes are the node features \mathbf{X} . The dataset comprises two half-moons representing two communities with 68% edges connecting them as bridge edges.

Explaining the Effectiveness of SGS-GNN on Heterophilic graph. Fig. 7 juxtaposes the input moon graph (Fig. 7, left) and the sparsified moon graph by SGS-GNN (Fig. 7, right). SGS-GNN removes a significant portion of bridge edges, causing an increase in edge homophily from 0.32 to 1.0. As a result, the accuracy of vanilla GCN increased from 80% on the full graph to 100% on the sparsified graph. Since heterophilous edges significantly hinder the node representation learning, SGS-GNN identifies them during training and learns to put less probability mass on such edges for downstream node classification. Due to this learning dynamics, SGS-GNN is more effective on heterophilic graphs such as the Moon graph.

Original dense graph with training nodes highlighted

Learned sparse subgraph with 20% edges



Figure 7: Toy example with two half moon demonstrates the effectiveness of SGS-GNN. The original graph has 68% edges with different node labels; in contrast, the learned sparse subgraph from SGS-GNN contains no such bridge edges.

C Additional algorithmic details of SGS-GNN

Conditional update of EdgeMLP. Backward propagation is often the most computationally intensive part of training, so we employ a conditional mechanism to update EdgeMLP selectively. We evaluate the learned sparse subgraph (line 9, Alg. 3) against a subgraph from the prior probability distribution p_{prior} (line 11, Alg. 3). If the training F1-score from the learned sparse subgraph is better than the baseline, parameters of EdgeMLP are updated (line 19, Alg. 3). Otherwise, the update to EdgeMLP is skipped (line 22, Alg. 3).

The detailed algorithm for SGS-GNN with conditional updates is in Alg. 3.

Algorithm 3 SGS-GNN Training with conditional updates

```

1: Input:  $\mathcal{G}(\mathcal{V}, \mathcal{E}, \mathbf{X})$ , sample percent  $q$ , hops, METIS Parts,  $n$ 
2: Output: EdgeMLP, GNN
3: Compute  $p_{\text{prior}}(u, v) \leftarrow \frac{1/d_u + 1/d_v}{\sum_{i,j \in \mathcal{E}} (1/d_i + 1/d_j)}$ 
4:  $\mathcal{G}_{\text{parts}} = \{\mathcal{G}_1, \mathcal{G}_2, \dots, \mathcal{G}_n\} \leftarrow \text{METIS}(\mathcal{G}(\mathcal{V}, \mathcal{E}, p), n)$ 
5: for epochs in max_epochs do
6:   for  $\mathcal{G}_i(\mathcal{V}_i, \mathcal{E}_i, \mathbf{X}_i, p_{\text{prior}}^i) \in \mathcal{G}_{\text{parts}}$  do
7:      $\tilde{p}, \mathbf{w} \leftarrow \text{EdgeMLP}(\mathcal{E}_i, p_{\text{prior}}^i, \mathbf{X}_i, \text{hops})$ 
8:      $\tilde{p}_a \leftarrow \lambda \tilde{p} + (1 - \lambda) p_{\text{prior}}^i$ 
9:      $\tilde{\mathcal{E}}, \tilde{\mathbf{w}} \leftarrow \text{Sample}(\tilde{p}_a, \mathbf{w}, \lfloor \frac{q|\mathcal{E}_i|}{100} \rfloor)$  /* Learned sparse subgraph */
10:     $\hat{\mathbf{Y}}, \hat{\mathbf{H}} \leftarrow \text{GNN}_{\theta}(\tilde{\mathcal{E}}, \tilde{\mathbf{w}}, \mathbf{X})$ 
11:     $\mathcal{E}_{\text{prior}} \leftarrow \text{Sample}(p_i, \lfloor \frac{q|\mathcal{E}_i|}{100} \rfloor)$  /* Sparse subgraph from prior */
12:     $\hat{\mathbf{Y}}_{\text{prior}} \leftarrow \text{GNN}_{\theta}(\mathcal{E}_{\text{prior}}, \mathbf{X})$ 
13:    if Evaluate( $\hat{\mathbf{Y}}$ )  $\geq$  Evaluate( $\hat{\mathbf{Y}}_{\text{prior}}$ ) then
14:       $\mathcal{L}_{\text{CE}} \leftarrow \text{CrossEntropy}(\mathbf{Y}_{\mathcal{V}_L}, \hat{\mathbf{Y}}_{\mathcal{V}_L})$ 
15:       $\forall_{(u,v) \in \mathcal{E}_i} u \in \mathcal{V}_L \wedge v \in \mathcal{V}_L : \text{mask}[u, v] \leftarrow \text{True}$ 
16:       $\mathcal{L}_{\text{assor}} \leftarrow \text{CrossEntropy}(\mathcal{E}[\text{mask}], \mathbf{w}[\text{mask}])$ 
17:       $\mathcal{L}_{\text{cons}} \leftarrow \text{Sim}(\mathbf{w}, \text{Cosine}(\mathbf{h}_u, \mathbf{h}_v) : \forall_{(u,v) \in \mathcal{E}})$ 
18:       $\mathcal{L} \leftarrow \alpha_1 \cdot \mathcal{L}_{\text{CE}} + \alpha_2 \cdot \mathcal{L}_{\text{assor}} + \alpha_3 \cdot \mathcal{L}_{\text{cons}}$ 
19:      Backward Propagate through  $\mathcal{L}$  and optimize EdgeMLP $_{\phi}$ , GNN $_{\theta}$ .
20:    else
21:       $\mathcal{L}_{\text{CE}} \leftarrow \text{CrossEntropy}(\mathbf{Y}_{\mathcal{V}_L}, \hat{\mathbf{Y}}_{\mathcal{V}_L})$ 
22:      Backward Propagate through  $\mathcal{L}_{\text{CE}}$  and optimize GNN $_{\theta}$ .
23:    end if
24:  end for
25: end for
26: Return EdgeMLP, GNN

```

Inference. During inference, we use the learned probability distribution from `EdgeMLP`. We keep track of the best temperature T that gave the best validation accuracy and use that to sample an ensemble of sparse subgraphs. Then, we mean-aggregate their representations to produce the final prediction on a test node.

The reason we consider ensemble of subgraphs is because there are variability in the edges of the sample subgraphs even if they are all sampled from the same distribution. Thus mean-aggregation of node embeddings is an effective way to improve the robustness of the learned node embeddings.

The inference pseudocode is provided in Algorithm 4.

Algorithm 4 SGS-GNN Inference

```

1: Input: Graph  $\mathcal{G}(\mathcal{V}, \mathcal{E}, \mathbf{X})$ , sample %  $q$ , Ensemble size,  $R$ .
2: Output: Prediction,  $\hat{\mathbf{Y}}$ 
3:  $\mathbf{w}, \tilde{p} = \text{EdgeMLP}(\mathcal{E}, \mathbf{X}, T_{\text{best}})$  /* Use  $T$  that gave best validation accuracy. */
4:  $S_y \leftarrow \emptyset$  /* Predictions */
5: for  $i$  in  $R$  do
6:    $\tilde{\mathcal{E}}, \tilde{\mathbf{w}} \leftarrow \text{Sample}(\tilde{p}, \lfloor \frac{q|\mathcal{E}|}{100} \rfloor)$ 
7:    $\hat{\mathbf{Y}}_i \leftarrow \text{GNN}_\theta(\tilde{\mathcal{E}}, \tilde{\mathbf{w}}, \mathbf{X})$ 
8:    $S_y \leftarrow S_y \cup \hat{\mathbf{Y}}_i$ 
9: end for
10: Predict,  $\hat{\mathbf{Y}} \leftarrow \text{Mean}(S_y)$ 
11: Return  $\hat{\mathbf{Y}}$ 

```

D Dataset Description

Table 4: Additional details of the dataset are provided. \mathcal{H}_{adj} refers to adjusted homophily. d corresponds to the average degree, C number of classes, and F is the feature dimension. Tr is the training label rate.

DATASET	$ \mathcal{V} $	$ \mathcal{E} $	d	\mathcal{H}_{adj}	C	F	TR.	SELF-LOOP	ISOLATED	CONTEXT
CORNELL	183	557	3.04	-0.42	5	1703	0.48	TRUE	FALSE	WEB PAGES
TEXAS	183	574	3.14	-0.26	5	1703	0.48	TRUE	FALSE	WEB PAGES
WISCONSIN	251	916	3.65	-0.20	5	1703	0.48	TRUE	FALSE	WEB PAGES
REED98	962	37,624	39.11	-0.10	3	1001	0.6	FALSE	FALSE	SOCIAL NETWORK
AMHERST41	2,235	181,908	81.39	-0.07	3	1193	0.6	FALSE	FALSE	SOCIAL NETWORK
PENN94	41,554	2,724,458	65.56	-0.06	2	4814	0.47	FALSE	FALSE	SOCIAL NETWORK
ROMAN-EMPIRE	22,662	65,854	2.91	-0.05	18	300	0.5	FALSE	FALSE	WIKIPEDIA
CORNELL5	18,660	1,581,554	84.76	-0.04	3	4735	0.6	FALSE	FALSE	WEB PAGES
SQUIRREL	5,201	396,846	76.30	-0.01	5	2345	0.48	TRUE	FALSE	WIKIPEDIA
JOHNSHOPKINS55	5,180	373,172	72.04	0.00	3	2406	0.6	FALSE	FALSE	WEB PAGES
ACTOR	7,600	53,411	7.03	0.01	5	932	0.48	TRUE	FALSE	ACTORS IN MOVIES
MINESWEEPER	10,000	78,804	7.88	0.01	2	7	0.5	FALSE	FALSE	SYNTHETIC
QUESTIONS	48,921	307,080	6.28	0.02	2	301	0.5	FALSE	FALSE	YANDEX Q
CHAMELEON	2,277	62,792	27.58	0.03	5	2581	0.48	TRUE	FALSE	WIKI PAGES
TOLOKERS	11,758	1,038,000	88.28	0.09	2	10	0.5	FALSE	FALSE	TOLOKA PLATFORM
AMAZON-RATINGS	24,492	186,100	7.60	0.14	5	556	0.5	FALSE	FALSE	CO-PURCHASE NETWORK
GENIUS	421,961	1,845,736	4.37	0.17	2	12	0.6	FALSE	TRUE	SOCIAL NETWORK
POKEC	1,632,803	44,603,928	27.32	0.42	3	65	0.6	FALSE	FALSE	SOCIAL NETWORK
ARXIV-YEAR	169,343	2,315,598	13.67	0.26	5	128	0.6	FALSE	FALSE	CITATION
SNAP-PATENTS	2,923,922	27,945,092	9.56	0.21	5	269	0.6	TRUE	TRUE	CITATION
OGBN-PROTEINS	132,534	79,122,504	597.00	0.05	94	8	0.2	FALSE	FALSE	PROTEIN NETWORK
CORA	19,793	126,842	6.41	0.56	70	8710	0.2	FALSE	FALSE	CITATION NETWORK
DBLP	17,716	105,734	5.97	0.68	4	1639	0.2	FALSE	FALSE	CITATION NETWORK
COMPUTERS	13,752	491,722	35.76	0.68	10	767	0.6	FALSE	TRUE	CO-PURCHASE NETWORK
PUBMED	19,717	88,648	4.50	0.69	3	500	0.2	FALSE	FALSE	SOCIAL NETWORK
CORA_ML	2,995	16,316	5.45	0.75	7	2879	0.2	FALSE	FALSE	CITATION NETWORK
SMALLCORA	2,708	10,556	3.90	0.77	7	1433	0.05	FALSE	FALSE	CITATION NETWORK
CS	18,333	163,788	8.93	0.78	15	6805	0.2	FALSE	FALSE	CO-AUTHOR NETWORK
PHOTO	7,650	238,162	31.13	0.79	8	745	0.2	FALSE	TRUE	CO-PURCHASE NETWORK
PHYSICS	34,493	495,924	14.38	0.87	5	8415	0.2	FALSE	FALSE	CO-AUTHOR NETWORK
CITSEER	4,230	10,674	2.52	0.94	6	602	0.2	FALSE	FALSE	CITATION NETWORK
WIKI	11,701	431,726	36.90	0.58	10	300	0.99	TRUE	TRUE	WIKIPEDIA
REDDIT	232,965	114,615,892	491.99	0.74	41	602	0.66	FALSE	FALSE	SOCIAL NETWORK

Table 4 shows the details of the characteristics of the graph datasets, including the splits used throughout the experimentation.

Along with synthetic dataset, for heterophily, we used, *Cornell*, *Texas*, *Wisconsin* from the *WebKB* (Pei et al., 2020); *Chameleon*, *Squirrel* (Rozemberczki et al., 2021); *Actor* (Pei et al., 2020); *Wiki*, *ArXiv-year*, *Snap-Patents*, *Penn94*, *Pokec*, *Genius*, *reed98*, *amherst41*, *cornell5*, and *Yelp* (Lim et al., 2021). We also experiment on some recent benchmark datasets, *Roman-empire*, *Amazon-ratings*, *Minesweeper*, *Tolokers*, and *Questions* from (Platonov et al., 2023).

For homophily, we used *Cora* (Sen et al., 2008); *Citeseer* (Giles et al., 1998); *pubmed* (Namata et al., 2012); *Coauthor-cs*, *Coauthor-physics* (Shchur et al., 2018); *Amazon-computers*, *Amazon-photo* (Shchur et al., 2018); *Reddit* (Hamilton et al., 2017); and, *DBLP* (Fu et al., 2020).

Heterophily Characterization. The term *homophily* in a graph describes the likelihood that nodes with the same labels are neighbors. Although there are several ways to measure homophily, three commonly used measures are *homophily of the nodes* (\mathcal{H}_n), *homophily of the edges* (\mathcal{H}_e), and *adjusted homophily* (\mathcal{H}_{adj}). The *node homophily* (Pei et al., 2020) is defined as,

$$\mathcal{H}_n = \frac{1}{|\mathcal{V}|} \sum_{u \in \mathcal{V}} \frac{|\{v \in \mathcal{N}(u) : y_v = y_u\}|}{|\mathcal{N}(u)|}. \quad (20)$$

The *edge homophily* (Zhu et al., 2020) of a graph is,

$$\mathcal{H}_e = \frac{|\{(u, v) \in \mathcal{E} : y_u = y_v\}|}{|\mathcal{E}|}. \quad (21)$$

The *adjusted homophily* (Platonov et al., 2022) is defined as,

$$\mathcal{H}_{\text{adj}} = \frac{\mathcal{H}_e - \sum_{k=1}^c \frac{D_k^2}{2|\mathcal{E}|^2}}{1 - \sum_{k=1}^c \frac{D_k^2}{2|\mathcal{E}|^2}}. \quad (22)$$

Here, $D_k = \sum_{v: y_v=k} d_v$ denote the sum of degrees of the nodes belonging to class k .

The values of the node homophily and the edge homophily range from 0 to 1, and the adjusted homophily ranges from $-\frac{1}{3}$ to +1 (Proposition 1 in (Platonov et al., 2022)). Among these measures, adjusted homophily considers the class imbalance. Thus, this work classifies graphs with adjusted homophily, $\mathcal{H}_{\text{adj}} \leq 0.50$ as heterophilic.

E Runtime Comparison

E.1 Impact of Conditional Updates on Runtime

Table 5 compares the runtime of SGS-GNN with and without conditional updates for large-scale graphs (with $|\mathcal{E}| \geq 1M$). The results indicate that conditional updates are similar to our standard training algorithm in terms of computational efficiency while providing improvements in F1-score under identical conditions. The additional computational costs of evaluation with prior get compensated by fewer updates of EdgeMLP.

Table 5: Comparison of runtime of SGS-GNN with and without conditional updates on large-scale graphs (with $|\mathcal{E}| \geq 1M$). Here, *Runtime (s)* refers to the mean training time per epoch. The terms EdgeMLP/GNN represent the proportion of time the EdgeMLP module is updated relative to the GNN. The results indicate that conditional updates are not significantly slower than our standard training algorithm, yet provide performance improvements to SGS-GNN under similar conditions.

DATASET	NODE	EDGES	DEGREE	SGS-GNN RUNTIME (S)		SGS-GNN F1-SCORE		#EDGEMLP/#GNN
				W/O. COND	W. COND	W/O. COND	W. COND	
CORNELL5	18,660	1,581,554	84.76	0.3625	0.3795	69.02 ± 0.09	69.12 ± 0.20	0.94
TOLOKERS	11,758	1,038,000	88.28	0.1743	0.1630	78.12 ± 0.13	78.13 ± 0.17	0.42
GENIUS	421,961	1,845,736	4.37	0.3884	0.4799	79.92 ± 0.08	80.07 ± 0.11	0.43
POKEC	1,632,803	44,603,928	27.32	6.7984	6.4885	62.05 ± 0.33	62.20 ± 0.10	0.75
ARXIV-YEAR	169,343	2,315,598	13.67	0.4571	0.4580	36.99 ± 0.11	36.98 ± 0.13	0.23
SNAP-PATENTS	2,923,922	27,945,092	9.56	6.3470	7.1236	34.86 ± 0.15	34.95 ± 0.16	0.84
REDDIT	232,965	114,615,892	491.99	8.0892	8.2960	91.45 ± 0.07	91.43 ± 0.02	0.44

E.2 Comparison with Baseline GNN based Sparsifiers

Table 6 shows related algorithms’ mean training time (s). Although SGS-GNN is slower than the unsupervised sparsification-based GNNs, it is significantly faster than supervised sparsifiers.

Table 6: Mean training time (s) per epoch of related methods. OOM refers to out-of-memory.

METHOD	CLUSTERGCN	GRAPHSAINTE	DROPEGE	MOG	SPARSEGAT	NEURAL SPARSE	SGS-GNN
CS	0.0095	0.0089	0.0146	OOM	0.1009	0.1515	0.0221
QUESTIONS	0.0082	0.0072	0.0290	0.1263	0.0236	0.1221	0.0261
AMAZON-RATINGS	0.0068	0.0062	0.0169	0.1054	0.0152	0.0499	0.0178
JOHNSHOPKINS55	0.0071	0.0061	0.0207	OOM	0.0102	0.1234	0.0244
AMHERST41	0.0062	0.0058	0.0101	OOM	0.0053	0.0368	0.0162

F Ablation Studies

This section investigates how different components of SGS-GNN behave and contribute to overall performance. We organize this section as follows,

1. Section F.1 investigates $\mathcal{L}_{\text{assor}}$, $\mathcal{L}_{\text{cons}}$, EdgeMLP, GNN, and Conditional Updates mechanism. We also compare its runtime against standard SGS-GNN training vs SGS-GNN with conditional updates. We also show SGS-GNN can be used with other GNNs in Sec F.1.1.
2. Section F.2 explores parameter settings with/without prior, different normalization and sampling methods, and inference with/without an ensemble of subgraphs.
3. Section F.3 shows ideal settings for regularizer coefficients $\alpha_1, \alpha_2, \alpha_3$. We also show the impact of λ for augmenting the learned probability distribution p using p_{prior} .

F.1 $\mathcal{L}_{\text{assor}}$, $\mathcal{L}_{\text{cons}}$, EdgeMLP, GNN, and Conditional Updates

Table 7 illustrates the performance of SGS-GNN with various combinations of regularizers, embedding layers in EdgeMLP, and convolutional layers in GNN.

1. $\mathcal{L}_{\text{assor}}$: Case 1, 2 shows improvement in results when $\mathcal{L}_{\text{assor}}$ is used.
2. $\mathcal{L}_{\text{cons}}$: From cases 4, 6, 8 shows L_{cons} improves results when GCN module is used in the GNN.
3. EdgeMLP: In general, we found that the GCN layers for EdgeMLP encodings performs best (cases 5-6, 11-12).
4. GNN: Both GCN and GAT modules yielded overall the best results (case 6, 11).
5. Conditional updates: Case 3 shows that conditional updates can benefit some graphs.

We also investigated the runtime and quality of SGS-GNN with and without conditional updates for large-scale graphs. We found both have similar runtime as the condition check expense gets compensated by fewer updates of EdgeMLP. Detailed comparisons of conditional updates in large graphs ($|\mathcal{E}| \geq 1M$) are included in the Table 5.

Table 7: Combination of EdgeMLP, GNN, Conditional update and L_{cons} .

	L_{assor}	L_{cons}	EDGEMLP	GNN	COND.	SMALLCORA	CORAFULL	JOHNSHOPKIN
1	N	N	MLP	GCN	N	73.80 ± 0.67	61.78 ± 0.20	66.12 ± 1.38
2	Y	N	MLP	GCN	N	74.88 ± 0.15	63.99 ± 0.24	66.18 ± 1.05
3	Y	N	MLP	GCN	Y	75.82 ± 0.46	64.07 ± 0.31	66.87 ± 0.93
4	Y	Y	MLP	GCN	Y	76.58 ± 0.47	65.33 ± 0.28	69.25 ± 0.76
5	Y	N	GCN	GCN	Y	75.80 ± 0.77	65.66 ± 0.14	71.06 ± 0.32
6	Y	Y	GCN	GCN	Y	77.50 ± 0.62	66.56 ± 0.22	70.79 ± 0.18
7	Y	N	GSAGE	GCN	Y	75.82 ± 0.44	63.70 ± 0.09	67.53 ± 0.80
8	Y	Y	GSAGE	GCN	Y	77.48 ± 0.61	65.12 ± 0.11	68.63 ± 0.66
9	Y	N	MLP	GAT	Y	77.72 ± 1.63	66.40 ± 0.08	67.92 ± 0.73
10	Y	Y	MLP	GAT	Y	75.78 ± 3.22	66.46 ± 0.16	68.17 ± 0.33
11	Y	N	GCN	GAT	Y	78.18 ± 0.74	66.33 ± 0.20	71.97 ± 0.59
12	Y	Y	GCN	GAT	Y	76.94 ± 2.76	66.39 ± 0.18	71.00 ± 0.96
13	Y	N	GSAGE	GAT	Y	77.98 ± 0.79	66.38 ± 0.23	69.29 ± 1.56
14	Y	Y	GSAGE	GAT	Y	75.74 ± 2.02	66.41 ± 0.25	68.82 ± 0.24

F.1.1 SGS-GNN WITH OTHER GNN MODULES

The sampled sparse subgraphs from EdgeMLP can be fed into any downstream GNNs and demonstrate a couple of variants of SGS-GNN. Chebnet from Chebyshev (He et al., 2022), Graph Attention Network (GAT) (Veličković et al., 2017), Graph Isomorphic Network (GIN) (Xu et al., 2018), Graph Convolutional Network (GCN) (Kipf & Welling, 2016) are some of the GNNs used for demonstration.

Fig. 8 shows the performance of these GNNs on homophilic and heterophilic datasets. SGS-GCN and SGS-GAT are two best performing models.

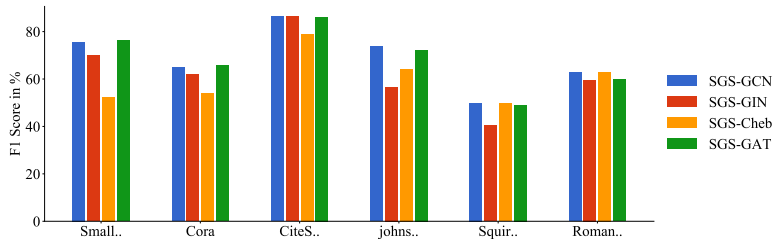


Figure 8: Performance of SGS-GNN with different GNN modules using 20% edges.

Table 8: Ablation Studies different components of SGS-GNN.

CASE	PRIOR	NORM.	SAMPL.	ENSEM.	SMALLCORA	CORA_ML	CITESEER	SQUIRREL	JOHNSHOPKINS55	ROMAN-EMPIRE
1	N	SUM	MULT	N	69.30 ± 1.20	81.05 ± 0.74	82.84 ± 0.47	48.90 ± 1.06	63.86 ± 0.58	63.27 ± 0.31
2	N	SUM	MULT	Y	72.84 ± 0.91	82.92 ± 0.73	87.42 ± 0.42	46.30 ± 1.18	65.14 ± 1.14	64.31 ± 0.13
3	Y	SUM	MULT	Y	75.54 ± 0.41	83.87 ± 0.69	86.31 ± 0.26	47.97 ± 0.60	72.68 ± 0.51	62.88 ± 0.19
4	Y	SOFTMAX	MULT	Y	75.44 ± 0.51	83.81 ± 0.72	86.31 ± 0.26	47.90 ± 0.42	72.97 ± 0.20	62.98 ± 0.16
5	Y	GUMBEL	TOPK	Y	76.24 ± 0.43	83.36 ± 0.34	86.44 ± 0.16	51.49 ± 0.72	71.83 ± 1.00	63.00 ± 0.11

PRIOR: USE OF PRIOR, **SUM:** SUM-NORMALIZATION, **SOFTMAX:** Softmax WITH TEMPERATURE ANNEALING
MULT: Multinomial SAMPLING, **GUMBEL:** Gumbel-Softmax WITH TopK

F.2 Impact of p_{prior} , Normalization & Sampling schemes, and Ensembling on SGS-GNN

Table 8 highlights the impact of the following components:

1. Prior p_{prior} : Cases 2-3 show that augmenting the learned probability distribution \tilde{p} with prior p_{prior} can benefit some datasets. We have also conducted an in-depth comparison between the distributions \tilde{p} and augmented distribution \tilde{p}_a . Figure 9 shows that there \tilde{p}_a is left skewed whereas \tilde{p} is not. Since rare edges still get some negligible mass, it is possible for \tilde{G} constructed from \tilde{p}_a to retain some bridge edges from these tails, if there are any.

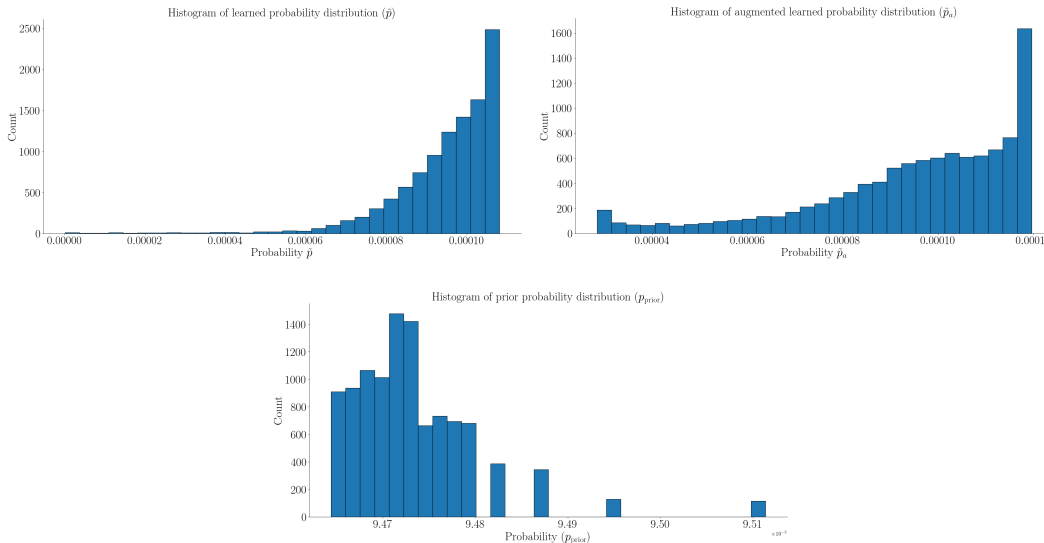


Figure 9: The learned probability distribution \tilde{p} (top-left), augmented distribution \tilde{p}_a (top-right) and fixed prior p_{prior} (bottom). Augmentation puts negligible mass on some rare yet critical edges in the left tail of \tilde{p}_a .

2. Normalization and Sampling: We considered three normalization and sampling techniques. i) sum-normalization with multinomial sampling, ii) softmax-normalization with temperature with multinomial sampling, and iii) Gumbel softmax normalization with Topk selection. Cases 3-5 show that each of these techniques can improve results in certain datasets, and thus, it is difficult to nominate a single one as best. However, in our experiments, we opted for multinomial sampling with softmax temperature annealing for training to encourage exploration in early iterations.
3. Ensemble subgraphs during inference: Case 2 demonstrates that using multiple subgraphs for ensemble prediction yields better results than a single subgraph (Case 1).

E.3 Choosing Values for Regularizer coefficient α_3 and Parameter λ

Recall that SGS-GNN computes the total loss at each epoch as

$$\mathcal{L} = \alpha_1 \mathcal{L}_{CE} + \alpha_2 \mathcal{L}_{assor} + \alpha_3 \mathcal{L}_{cons},$$

where $0 \leq \alpha_1, \alpha_2, \alpha_3 \leq 1$ are regularizer coefficients corresponding to the cross-entropy loss \mathcal{L}_{CE} , assortativity loss L_{assor} and consistency loss \mathcal{L}_{cons} respectively.

Also recall that, when we use a prior probability distribution, the learned distribution values of \tilde{p} are weighted through λ in $\tilde{p} = \lambda \hat{p} + (1 - \lambda)p_{prior}$

To avoid numerous combinations of values of three coefficients + the parameter λ , we have fixed $\alpha_1 = 1$, and $\alpha_2 = 1$. In the following, we investigate the performance of SGS-GNN with different values for α_3 and λ .

Fig. 10 shows a grid search for different combinations of λ and α_3 . As per our observation, the recommended values are $\lambda \in [0.3, 0.7], \alpha_3 = 0.5$.

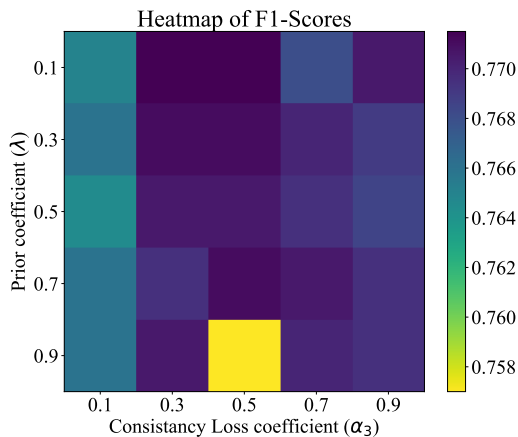


Figure 10: Grid search for the parameter λ for prior, and consistency loss, α_3 (Cora dataset).